Ore Geology Reviews 129 (2021) 103939

Contents lists available at ScienceDirect

Ore Geology Reviews

journal homepage: www.elsevier.com/locate/oregeorev

Accumulation of sulfides in the basement of southern Hunan Province, China: Implications for Pb–Zn mineralization related to reduced granitoids

Teng Ding [a,b,c,*], Jia Wang [a], Tingting Tan [a], Dongsheng Ma [b], Jianjun Lu [b], Rongqing Zhang [b], Jin Liang [c], Chuanwei Zhu [d], Bin Wu [e]

[a] Institute of Marine Geology, College of Oceanography, Hohai University, Nanjing 210098, China
[b] State Key Laboratory for Mineral Deposits Research, Nanjing University, Nanjing 210046, China
[c] Key Laboratory of Submarine Geosciences, Second Institute of Oceanography, Ministry of Natural Resources, Hangzhou 310012, China
[d] State Key Laboratory of Ore Deposit Geochemistry (SKLODG), Institute of Geochemistry, Chinese Academy of Sciences, Guiyang 550002, China
[e] State Key Laboratory of Nuclear Resources and Environment, East China University of Technology, Nanchang 330013, China

ARTICLE INFO

Keywords:
Huangshaping
Pb–Zn mineralization
Granitoids
Granodioritic enclaves
Sulfide

ABSTRACT

Southern Hunan Province lies at the intersection of the Shi–Hang zone and Nanling belt, and is characterized by extensive Mesozoic igneous rocks and coeval polymetallic deposits, including early granodiorite porphyry-related Cu–Pb–Zn polymetallic mineralization (ca. 160 Ma) and late granite-related W–Sn polymetallic mineralization (ca. 155 Ma). Amongst these deposits, the Huangshaping deposit is unique for the coexistence of economic W–Mo and Pb–Zn mineralization, which is associated with reduced granitoids, including quartz porphyry, felsite, and granite porphyry. Unlike the W–Mo mineralization, which has a close temporal–spatial relationship with granite porphyry, the sources of Pb–Zn mineralization have not yet been clarified, mainly because of its distal orebodies of unknown age. Abundant granodioritic enclaves have recently been found in quartz porphyry of the Huangshaping deposit, with zircon U–Pb ages consistent with the quartz porphyry and containing abundant sulfides including chalcopyrite, sphalerite, and pyrrhotite. This study involved *in situ* LA–ICP–MS determinations of trace element compositions of these sulfides, for comparison with those of sulfides in distal ores and carbonate strata to elucidate the sources of Pb–Zn mineralization in this deposit. Sulfides from granodioritic enclaves have higher Co/Ni ratios, but similar Zn/Cd, Cu/In, and Pb/Sb ratios, compared with those of distal Pb–Zn ores, indicating that sulfides in both enclaves and ores were precipitated from hydrothermal fluids derived from the same single source, although with higher precipitation temperatures for the former. As sulfides in the ores have Pb isotopic compositions distinct from those of other granitoids, we suggest that intrusion of the granodiorites (~5 Myrs before the granitoids) resulted in the accumulation of ore-forming metals in the metamorphic or crystalline basement. These metals were then scavenged by hydrothermal circulation triggered by later intrusions of felsite and granite porphyry, especially fluorine-rich granite porphyry, forming the distal Pb–Zn mineralization near the surface of the deposit. The accumulation of sulfides triggered by earlier granodioritic activity was likely crucial for the formation of distal sulfide mineralization, and perhaps also for that in other W–Mo deposits related to reduced granites in southern Hunan Province.

1. Introduction

Skarn Pb–Zn sulfide mineralization can develop in a variety of magmatic systems, regardless of geological environment and the type and redox state of related igneous rocks (Ishihara, 1977, 1981; Large, 1992; Meinert et al., 2005). Unlike other skarn ores, which are generally located in proximal skarn zones (e.g., W, Sn, Mo, Fe, and Cu ores), the origins of skarn Pb–Zn mineralization are still under discussion, primarily because these sulfide ores are located within distal sedimentary carbonate-hosted stratiform orebodies with generally poor age constraints (Megaw et al., 1988; Meinert et al., 2005). Numerous studies have shown that the formation of skarn Pb–Zn mineralization is predominantly controlled by igneous rocks, as the ore-forming fluids have highly variable temperatures (100 °C–500 °C), but similar chemical characteristics as magmatic- rather than basinal-dominated fluids (Megaw et al., 1988; Samson et al., 2008; Kalender, 2011). Sulfide ores

* Corresponding author at: Institute of Marine Geology, College of Oceanography, Hohai University, Nanjing 210098, China.
E-mail address: dingteng16@hhu.edu.cn (T. Ding).

https://doi.org/10.1016/j.oregeorev.2020.103939
Received 6 June 2020; Received in revised form 1 December 2020; Accepted 12 December 2020
Available online 17 December 2020

also typically have consistent S and Pb isotopic compositions, similar to those of igneous rocks associated with this mineralization (Ault and Williams-Jones, 2004; Kalender, 2011; Li et al., 2012; Akiska et al., 2013; Shu et al., 2013; Wang et al., 2014; Xie et al., 2015; Ding et al., 2016a). However, other studies have shown that the isotopic compositions of sulfide ores (e.g., S and Pb) and fluid inclusions (e.g., O and H) can be variable in some cases, and proposed that metamorphosed basement, evaporitic sediments, and meteoric water have probably contributed significantly to Pb–Zn mineralization in skarn systems (Townley and Godwin, 2001; Oliver et al., 2006; Palinkaš et al., 2013; Hammerli et al., 2015a, 2015b; Ding et al., 2016b, 2016c).

Southern Hunan Province lies at the intersection of the Shi–Hang zone and Nanling belt, and is characterized by extensive Mesozoic igneous rocks and coeval polymetallic deposits, which include early granodiorite porphyry-related Cu–Pb–Zn polymetallic mineralization (*ca.* 160 Ma) and late granite-related W–Sn polymetallic mineralization (*ca.* 155 Ma) (Mao et al., 2013; Ding et al., 2015; Huang et al., 2017). In most of these W–Sn deposits, Pb–Zn mineralization of limited tonnage commonly occurs as distal orebodies, such as in the Xintianling (Zhang, 2014) and Xitian (Yao et al., 2013) skarn W deposits, and Hehuaping (Yao et al., 2014) and Xianghualing (Yuan et al., 2007) skarn Sn deposits. Although it is still difficult to figure out the key factors controlling the different W–Sn and Cu–Pb–Zn mineralization types, the redox states of ore-bearing igneous rocks are considered one of the most critical factors in the formation of economic Cu–Pb–Zn deposits in this area, mainly as chalcophile elements (e.g., S, Cu, Pb, and Zn) can be accumulated and transported more effectively in systems associated with relatively oxidized granodioritic magmas than in reduced W–Sn-bearing granitic magmas (Jiang et al., 2009; Zhang, 2014; Ding et al., 2015; Huang et al., 2017).

The polymetallic Huangshaping W–Mo–Pb–Zn deposit hosts significant W–Mo and Pb–Zn mineralization—a combination that is unique in southern Hunan Province—containing 152.9 kt WO_3 at a grade of 0.2%, 43.2 kt Mo at 0.2%, 761.3 kt Pb at 3.55%, and 1.5 Mt Zn at 7.13% (Huang et al., 2013). W–Mo mineralization in the deposit has close temporal–spatial relationships with granite porphyry, suggesting a genetic relationship between the two (Ding et al., 2017, 2018a, 2018b). However, the origins of the Pb–Zn mineralization within the deposit remain ambiguous, primarily as these sulfide ores are located within distal carbonate-hosted stratiform orebodies of unknown age, as in other Pb–Zn deposits (Ding et al., 2016b, 2016c). In addition, all granitoids (including quartz porphyry, felsite, and granite porphyry) in this deposit are reduced, as indicated by Ce(IV)/Ce(III) ratios in zircon (Li et al., 2014b) and the Fe(III)–Fe(II)–Mg discrimination diagram for biotite (Ding et al., 2017), distinct from the generally oxidized Cu–Pb–Zn-bearing granodiorite porphyry (Ding et al., 2015). Due to the apparent conflict between its large tonnage and the reduced states of associated granitoids, the formation mechanism of distal Pb–Zn mineralization in the Huangshaping deposit is still unclear (Tong, 1986; Xi et al., 2009; Zhu et al., 2012; Huang et al., 2013; Ding et al., 2016b, 2016c; Jiang et al., 2020; Li et al., 2020).

Abundant granodioritic enclaves were recently discovered within quartz porphyry of the Huangshaping deposit. They are geochemically similar to Cu–Pb–Zn-bearing granodiorite porphyries in southern Hunan Province rather than host-rock quartz porphyry of the deposit, indicating likely pre-existing (earlier than felsite and granite porphyry formation) granodioritic activity within the basement of the Huangshaping deposit (Ding et al., 2016c). Furthermore, these granodioritic enclaves contain numerous sulfides, including chalcopyrite, pyrrhotite, and sphalerite—assemblages that are absent in quartz porphyry, felsite, and granite porphyry in the deposit. Here we compare the trace element compositions of sulfides in the granodioritic enclaves and distal Pb–Zn ores hosted in sedimentary carbonate with the aims of (1) elucidating whether and how granodioritic activity may have contributed to Pb–Zn mineralization in the Huangshaping deposit and (2) improving understanding of distal Pb–Zn mineralization in other W–Sn deposits in southern Hunan Province.

2. Geological background

The Cathaysia Block amalgamated with the Yangtze Block along the Jiangshan–Shaoxin suture at *ca.* 970 Ma during the Jinning orogenic event (Li and McCulloch, 1996). The basement of the Cathaysia Block is dominated by Paleo- to Mesoproterozoic metamorphic rocks overlain by Neoproterozoic to Paleozoic continental and neritic marine sediments (Yuan et al., 1991; Wang et al., 2007; Jiang et al., 2009). The Cathaysia Block records intensive Jurassic–Cretaceous magmatism that formed a belt of igneous rocks that become younger towards the coast (Fig. 1a; Zhou et al., 2006). Intrusive and volcanic rocks of this period include a belt of granites with high Sm (>8 ppm) and Nd (>45 ppm) contents, $\varepsilon_{Nd}(t)$ values greater than − 8, and young Nd model ages ($T_{DM} < 1.5$ Ga; Gilder et al., 1996). This belt almost parallels two NE–SW-trending Mesozoic grabens between Hangzhou (Zhejiang Province) and Shiwandashan (Guangxi Province), and has thus been termed the Shi–Hang zone (Fig. 1a). Various models have been proposed for the formation of the Shi–Hang zone, including the commonly accepted models of shallow subduction and roll-back of the Paleo-Pacific Plate or the foundering of a flat-subducted slab with subsequent roll-back during the Jurassic (Li et al., 2007; Jiang et al., 2009; Ding et al., 2015).

The Shi–Hang zone is closely associated with Cu–Pb–Zn polymetallic deposits (Fig. 1a; Ding et al., 2015 and references therein). The area within Guangxi, Hunan, Jiangxi, and Guangdong provinces that contains W–Sn–Cu–Pb–Zn deposits associated with granitoids has been termed the Nanling belt (Fig. 1a; Mao et al., 2013). Southern Hunan Province lies within the Cathaysia Block, and igneous rocks within it and adjacent areas can be divided into granites formed by melting of crustal material and granodiorite porphyries formed from a mixture of crust- and mantle-derived materials. The former are associated with W–Sn polymetallic mineralization and the latter with skarn Cu–Pb–Zn polymetallic deposits such as the Baoshan (Xie et al., 2013, 2015; Ding et al., 2016b), Tongshanling (Huang et al., 2017, 2018), and Shuikoushan (Zuo et al., 2014) deposits (Fig. 1b). All these deposits are hosted by Devonian and Carboniferous carbonates, and the significant mineral endowment of southern Hunan Province means that this region has been the focus of considerable geological and mineral exploration and research (e.g., Hua et al., 2007; Li et al., 2013; Mao et al., 2013).

3. Geology of the Huangshaping deposit

3.1. Stratigraphy and structure

The Huangshaping deposit lies on the northwestern side of the Qitianling batholith (Fig. 1b). Sedimentary rocks of the deposit are predominantly neritic marine sediments, including limestones of the Upper Devonian Xikuangshan, Lower Carboniferous Douling'ao, and Shidengzi formations, Ceshui Formation sandstone, and Zimenqiao Formation dolomite and limestone (Fig. 2a, b). Shidengzi Formation limestone is the main host of W–Mo–Pb–Zn mineralization (Fig. 2c; Tong 1986). The dominant structure is the N–S-trending Guanyindazuo–Baoling inverted anticline, with a core of Shidengzi Formation rocks and limbs comprising the Ceshui and Zimenqiao formations (Fig. 2b, c). Three N–S-trending thrust faults (F1, F2, and F3) occur within the anticlinal axis and limbs (Fig. 2a). These faults, particularly F3, control the location of most of the Pb–Zn reserves (Fig. 2b, c). Several E–W- and WNW–ENE-trending normal faults (F0, F6, F7, and F9) occur within the deposit (Fig. 2a, b). The intersection of these faults and the anticline forms a crosshatch-shaped structure that controls both the outcrops of granitoids and locations of W–Mo–Pb–Zn mineralization.

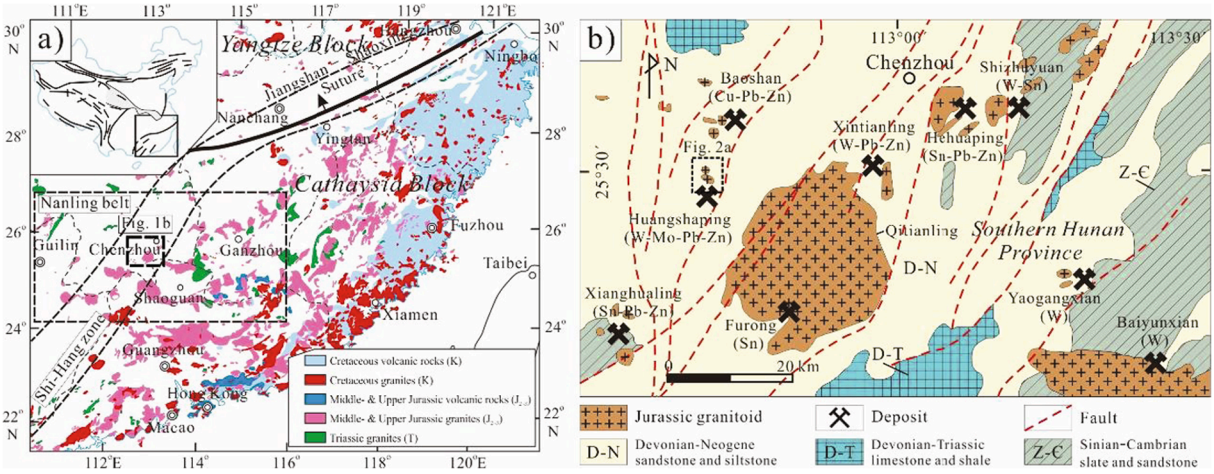

Fig. 1. (a) Distribution of Mesozoic intrusive and volcanic rocks in southeast China (modified from Zhou et al., 2006). Locations of the Shi–Hang zone and Nanling belt are from Jiang et al. (2009), Li et al. (2013), and Mao et al. (2013). (b) Distribution of Jurassic igneous rocks and associated polymetallic mineral deposits in southern Hunan Province, including the Huangshaping deposit.

3.2. Granitoids

3.2.1. Quartz porphyry, felsite, and granite porphyry

The Huangshaping deposit is associated with hypabyssal granitoids, which are divided into quartz porphyry, felsite, and granite porphyry, based on mineralogy, geochemistry, and texture. The mineral assemblage of the quartz porphyry is limited to quartz and minor K-feldspar phenocrysts. Felsite has an aphyric texture generally devoid of phenocrysts, and comprises monzogranite and syenogranite (Ding et al., 2016c). Granite porphyry contains K-feldspar, plagioclase, quartz, and minor biotite phenocrysts. Igneous rocks exposed in the deposit include quartz porphyry and weathered felsite, while granite porphyry occurs below the southeastern part of the deposit (Fig. 2b, c). The contacts between quartz porphyry and felsite are faults, but it is uncertain whether faulting caused intercalations of granite porphyry and other granitoids (Fig. 2b, c). All three types of granitoid contain similar accessory minerals, including primary zircon and apatite, and secondary sulfides and fluorite. Wolframite, columbite, and molybdenite also occur in the granite porphyry, suggesting a close relationship between granite porphyry and W–Mo mineralization in this deposit (Ding et al., 2017).

Previous studies have determined that the intrusions are silicic, with SiO_2 contents of >70 wt%. Their aluminum saturation index values of 0.7–1.6 indicate that the granitoids are metaluminous or peraluminous, and their K_2O contents of 3.7–7.0 wt% correspond to high-K calc-alkaline to shoshonitic igneous rocks (Yao et al., 2005; Li et al., 2014a; Ding et al., 2016c). Geochronological data indicate two periods of igneous activity, with quartz porphyry forming at 160.5 ± 1.3 Ma, and felsite and granite porphyry at 156.6 ± 1.4 and 155.3 ± 1.6 Ma, respectively (Ding et al., 2016c and references therein). Further support for distinct episodes of igneous activity is provided by Sr–Nd–Hf–Pb isotopic compositions, which indicate that the felsite and granite porphyry are co-magmatic and formed as a result of partial melting of metamorphic basement within the upper crust. In contrast, quartz porphyry associated with the Huangshaping deposit was formed by melting of metamorphic basement rocks within the lower crust, with coeval basaltic magma input (Li et al., 2014a; Ding et al., 2016c).

3.2.2. Granodioritic enclaves in quartz porphyry

Granodioritic enclaves occur in the quartz porphyry in the Huangshaping deposit, forming ellipsoidal or lens-shaped bodies with diameters of 5–40 cm (Fig. 3a, b). Some enclaves are strongly altered and have porphyritic textures with feldspar and quartz phenocrysts, and primary euhedral zircon and apatite are common accessory minerals (Ding et al., 2016c). Some enclaves are relatively fresh, with aphyric textures (Fig. 4a). Zircons from the granodioritic enclaves yield U–Pb ages of 160.2 ± 1.6 Ma, which is within error of the age of the host quartz porphyry (160.5 ± 1.3 Ma), indicating that the enclaves crystallized at the same time as the host quartz porphyry (Ding et al., 2016c). The two-stage Hf model ages, T^{C}_{DM}(Hf), of zircons from the enclaves are in the range 1.91–1.59 Ga, much older than those of quartz porphyry (1.61–1.32 Ga) and granite porphyry (1.72–1.42 Ga) (Ding et al., 2016c), but consistent with those of Pb–Zn-bearing granodiorite porphyries in the area, such as in the Tongshanling (1.83–1.65 Ga) (Jiang et al., 2009) and Baoshan (2.08–1.77 Ga) (Xie et al., 2013) deposits. Calculated rare earth element patterns of the granodioritic enclaves, based on their apatite contents, are similar to those of granodiorite porphyries in the area (e.g., the Tongshanling and Baoshan deposits), but distinct from those of granitoids in the Huangshaping deposit (Ding et al., 2016c). The granodioritic enclaves thus represent an end-member magma that was added to the quartz porphyry magma chamber, with this end-member magma being derived from melting of lower crust compositionally similar to that forming the Pb–Zn-bearing granodiorite porphyries in southern Hunan Province. It is particularly relevant that these granodioritic enclaves host abundant sulfides, including chalcopyrite, pyrrhotite, and sphalerite, which coexist in the enclaves forming discrete grains (Fig. 4a–e). These sulfides are distinct from secondary sulfides, which include mainly pyrite and generally occur as veinlets crosscutting granitoids (Fig. 4f–i; Ding et al., 2016b).

3.3. Alteration and mineralization

3.3.1. Skarn alteration

Skarn and sulfide–carbonate alteration characterize the Huangshaping deposit. Skarn occurs in a contact zone between granitoids and Shidengzi Formation limestones, with the most complete skarn development being around granite porphyry (Fig. 2b, c). Skarn alteration of limestone is zoned outward from potassic-altered granite porphyry to proximal garnet–diopside and tremolite. Sericitization with abundant arsenopyrite and minor scheelite also occurs in this potassic-altered granite porphyry (Fig. 5a, b). Disseminations of abundant scheelite and minor molybdenite are common in the proximal garnet–diopside skarn (Fig. 3c, d), which hosts significant W resources, including the No. W216 orebody that occurs close to the granite porphyry and contains 88% of known scheelite reserves in the deposit (Fig. 2b). The remaining 12% of reserves are in the No. W1 orebody, close to the quartz porphyry intrusion, but are considered closely associated with the felsite beneath (Fig. 2b; Ding et al., 2016b). The tremolite zone contains actinolite, abundant disseminated molybdenite, and minor scheelite (Fig. 3e).

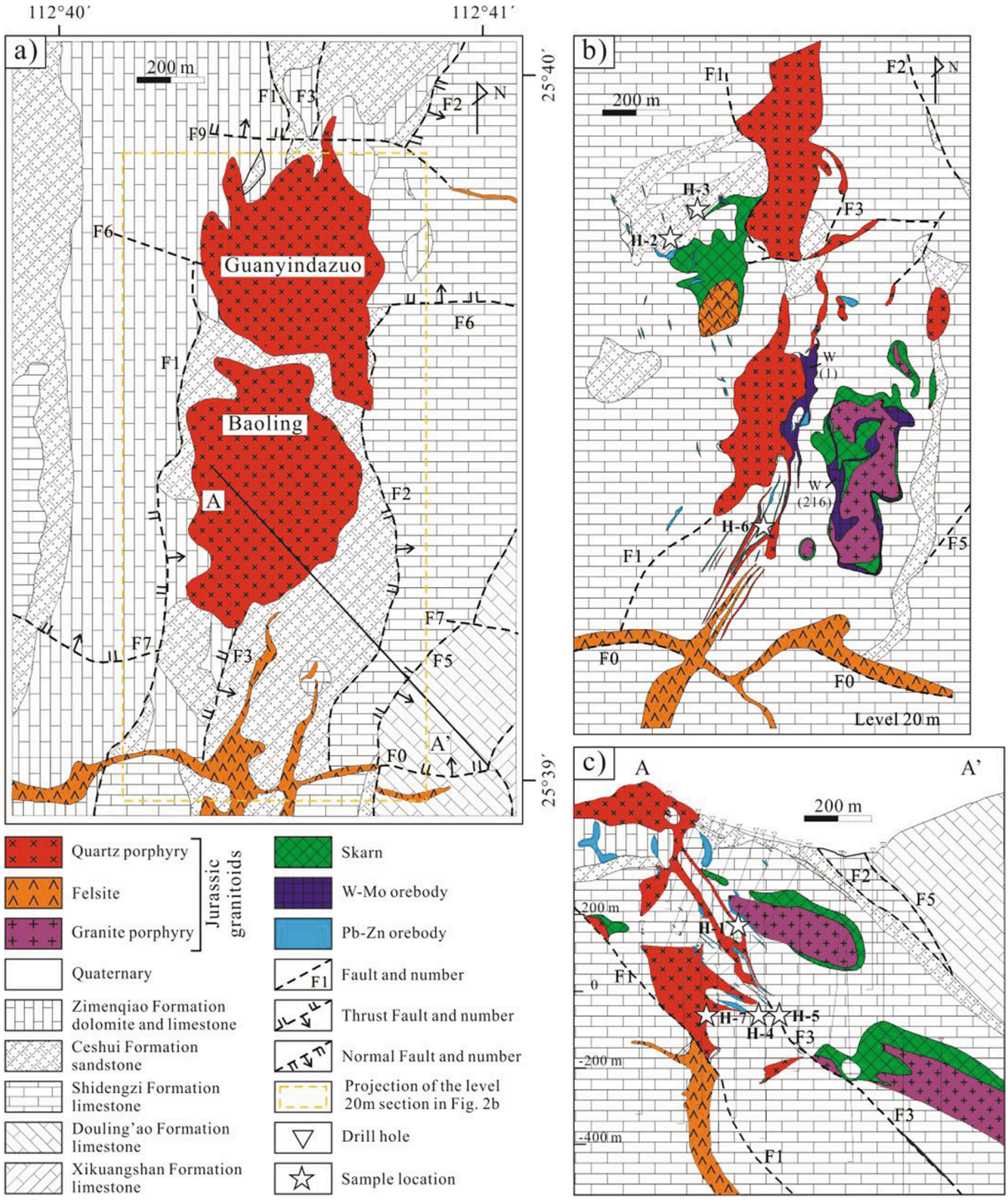

Fig. 2. (a) Geological map of the Huangshaping deposit; (b) simplified geological maps of the Huangshaping deposit at the 20 m level; (c) geological cross-section through the Huangshaping deposit. Stars in (b) and (c) represent the sampling locations of the sulfides analyzed in this study. Abbreviations H-1 to H-7 are short for 11HSP-26, −52, −55, −82, −99, −135, and 1212HSP14, respectively.

Calcite and fluorite are the main gangue minerals, crosscutting scheelite and molybdenite ores, and these can also host abundant scheelite and molybdenite (Fig. 3c–e and 5c–d). Fluid inclusions in garnet and disseminated scheelite and fluorite yield homogenization temperatures (T_h) of 528 °C–600 °C, 400 °C–460 °C, and 250 °C–303 °C, respectively (Huang et al., 2013; Li et al., 2016).

Sulfide–quartz mineralization in the Huangshaping deposit is weakly developed and commonly occurs as veinlets cutting skarn, while sulfide veinlets containing chalcopyrite, pyrite, and molybdenite cut early garnet and scheelite (Fig. 5e, f; Ding et al., 2016b). Fluid inclusions in quartz have T_h values of 300°–340 °C, lower than those of garnet and scheelite in proximal skarn (Huang et al., 2013; Li et al., 2016). Distal skarn is represented by a marble zone adjacent to unaltered limestone. The timing of skarn formation and mineralization is indicated by Re–Os isochron ages of 159.4 ± 3.3 to 153.8 ± 4.8 Ma for molybdenite in W–Mo skarn (Ma et al., 2007; Yao et al., 2007; Lei et al., 2010; Qi et al., 2012) and $^{40}Ar/^{39}Ar$ ages of 154.3 ± 0.6 to 152.9 ± 0.5 Ma for hydrothermal K-feldspar (Li et al., 2017). These ages are within analytical

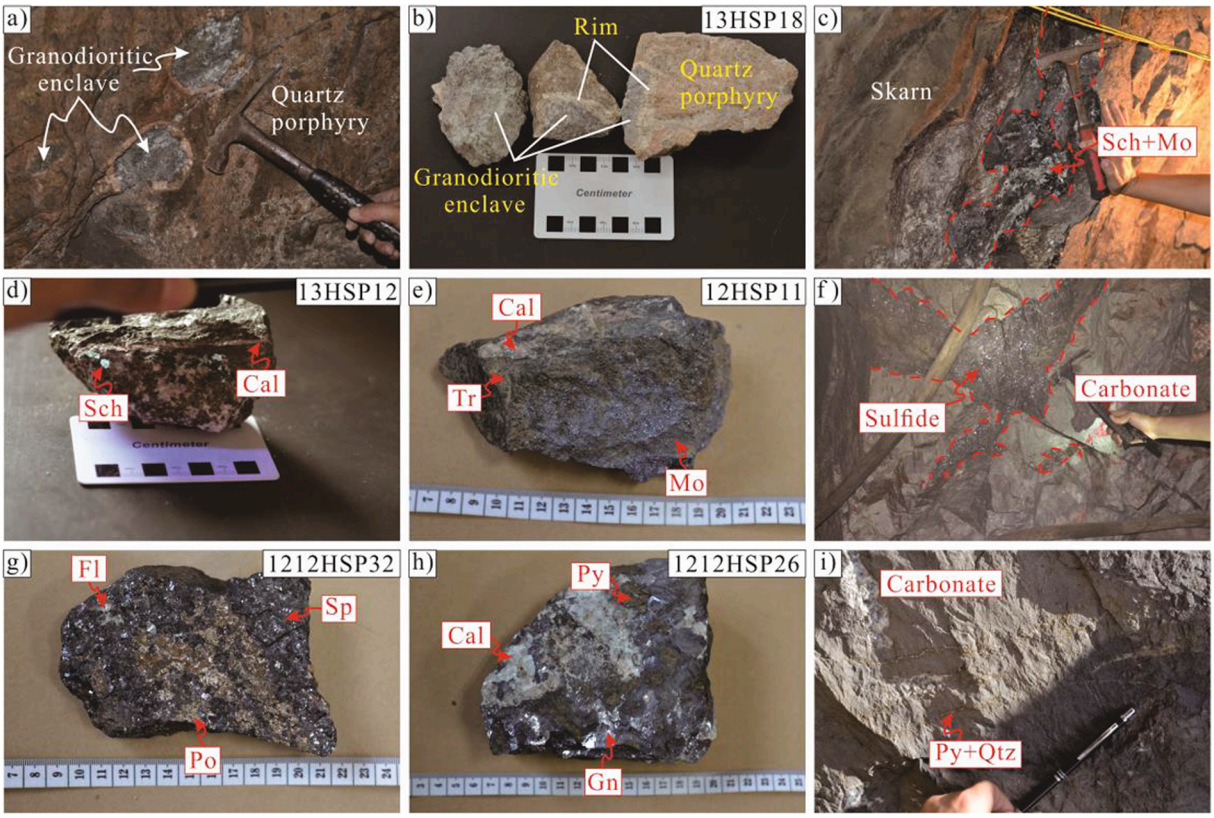

Fig. 3. (a) Ellipsoidal granodioritic enclaves with various diameters in the quartz porphyry; (b) hand specimens showing the clean reaction rims between granodioritic enclaves and quartz porphyry; (c) outcrop showing the scheelite–molybdenite orebody in the skarn zone; (d, e) hand specimens showing scheelite and molybdenite ores, respectively; (f) vein-type sulfide orebody hosted in distal sedimentary carbonate; (g) hand specimen showing sulfide ore comprising sphalerite and pyrrhotite, with fluorite gangue mineral; (h) hand specimen showing sulfide ore comprising galena and pyrite, with calcite gangue mineral; (i) carbonate strata cut by pyrite vein with quartz. Sch, scheelite; Mo, molybdenite; Cal, calcite; Tr, tremolite; Fl, fluorite; Po, pyrrhotite; Sp, sphalerite; Py, pyrite; Gn, galena; Qtz, quartz.

error of the 155.2 ± 0.4 Ma age of the granite porphyry (Yuan et al., 2014; Ding et al., 2016c), supporting a genetic relationship between the granite porphyry and W–Mo mineralization.

3.3.2. *Pb–Zn mineralization*

Pb–Zn mineralization formed during a sulfide–carbonate stage of mineralization, with this stage hosting almost all of the pyrrhotite, pyrite, sphalerite, and galena in the Huangshaping deposit. These sulfides are hosted by distal sedimentary carbonate, and occur as vein-type, stratiform, and lens-shaped zones of mineralization in Shidengzi Formation limestones, Ceshui Formation sandstones, and Zimenqiao Formation dolomitic limestones (Fig. 2c and 3f). The sulfide orebodies are located beneath hanging-wall rocks of Ceshui Formation sandstone and the quartz porphyry intrusion within the upper section of the Huangshaping deposit (Fig. 2b, c). The Pb–Zn orebodies within the same level of the deposit are not in contact (Fig. 2b), but are located along faults that acted as conduits for ore-forming fluids (Fig. 2c). Sulfide ores within the deposit are dominated by galena and sphalerite, with pyrrhotite and pyrite in a calcite and fluorite gangue (Fig. 3g, h). The Huangshaping deposit is zoned vertically, with the pyrrhotite abundance decreasing and pyrite abundance increasing upward within the deposit (Ding et al., 2016b).

Pyrrhotite is generally massive with minor coexisting chalcopyrite and sphalerite, indicating that these sulfides precipitated first in the ores (Fig. 5g). Pyrrhotite was then replaced by pyrite, sphalerite, and galena (Fig. 5g–i). Indeed, this sulfide can be completely replaced by pyrite, retaining pseudomorphic textures of pyrrhotite (Fig. 5i). Pyrite is more commonly colloform, surrounded by recrystallized pyrite (Fig. 5j). The abundance of colloform pyrite generally increased outwards in the sulfide ores from the granitoids to the strata, it can be easily distinguished from the recrystallized pyrite as its turbid appearance and concentric zonation. In addition to that coexisting with pyrrhotite, sphalerite can also replace pyrite in the sulfide ores (Fig. 5k), indicating that most sphalerite precipitated after pyrite, which in turn formed before galena (which generally replaced all the other sulfides) (Fig. 5h–k). Calcite and fluorite gangue minerals host fluid inclusions that homogenize at 160 °C–240 °C, with no obvious evidence of boiling (Huang et al., 2013). Pyrite grains and veins are disseminated or crosscut Shidengzi Formation limestones, indicative of sedimentary and hydrothermal pyrite, respectively (Fig. 5l–o). These samples were obtained from the unmineralized strata which are far away from the deposit. The paragenesis of most sulfides of the Huangshaping deposit is summarized in Fig. 6.

4. Methods

4.1. *Magnetic susceptibility analysis*

The low-frequency volumetric magnetic susceptibility of whole-rock sample powders (~5 cm^3) of granitoids from the Huangshaping deposit was measured using a Bartington Instruments (UK) MS2 magnetometer at the Ministry of Education Key Laboratory of Surficial Geochemistry, Nanjing University, Nanjing, China. The density magnetic susceptibility (SI) in 10^{-8} m^3 kg^{-1} was calculated by dividing the measured volumetric susceptibility by the sample weight, and SI/4π = mass magnetic susceptibility and 10^{-6} emu g^{-1} (CGS).

4.2. *In situ LA–ICP–MS analysis*

Different types of sulfide were selected on the basis of their paragenetic sequence and morphology for *in situ* laser ablation inductively

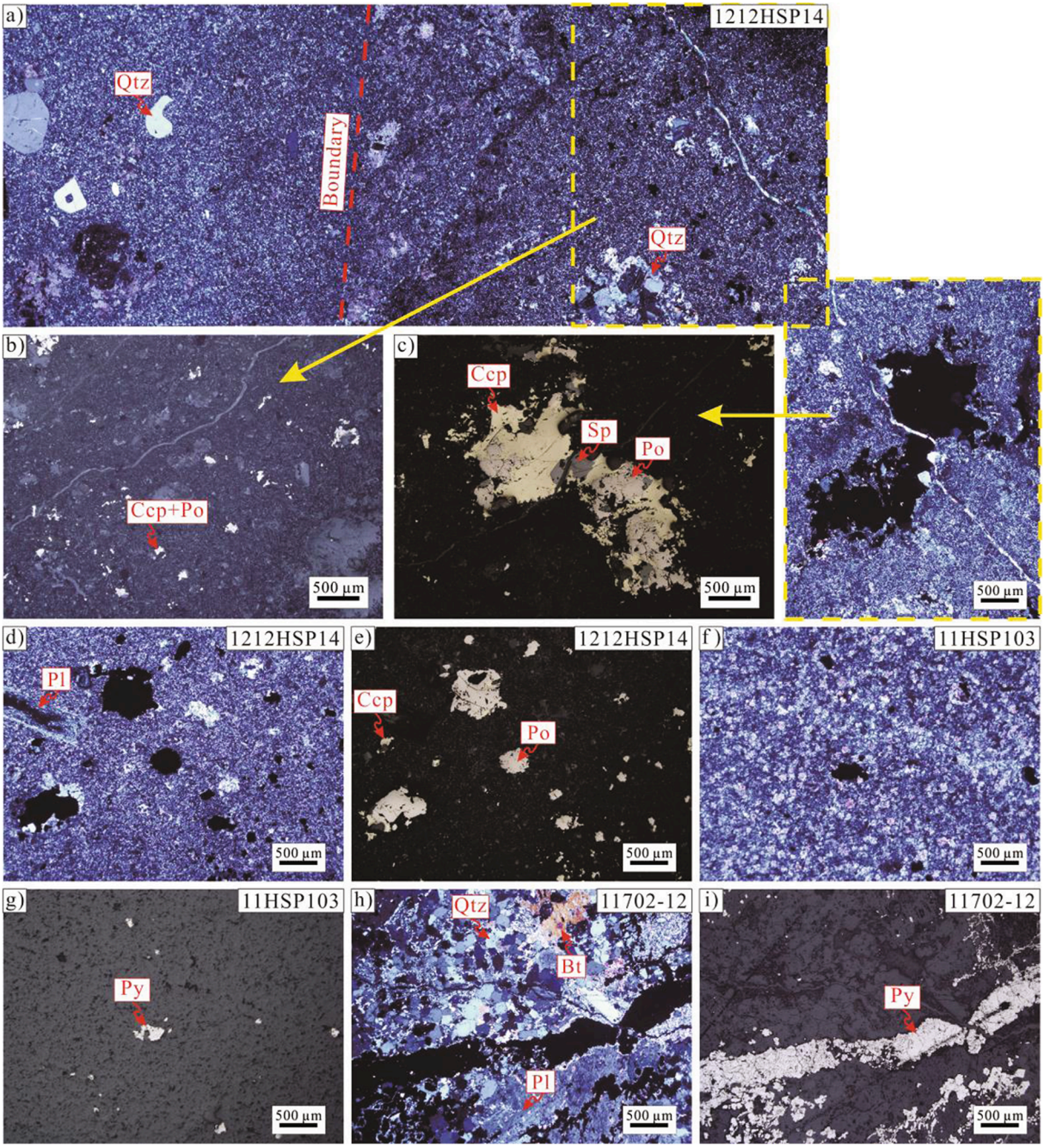

Fig. 4. Photomicrographs showing the occurrence of sulfides in granodioritic enclaves and granitoids of the Huangshaping deposit. (a) Contact zone between granodioritic enclaves and reaction rim (cross-polarized light (CPL)); (b–e) chalcopyrite, pyrrhotite, and sphalerite coexisting in granodioritic enclaves as discrete grains (b, c, e, reflected light (RL); d, CPL); (f, g) secondary pyrite in felsite (f, CPL; g, RL); (h, i) pyrite vein crosscutting granite porphyry (h, CPL; I, RL). Ccp, chalcopyrite; Pl, plagioclase; Bt, biotite; other abbreviations as in Fig. 3.

coupled plasma mass spectrometry (LA–ICP–MS) analysis of trace element compositions, using a New Wave UP-213 Nd:YAG LA system coupled to a Bruker Aurora M90 ICP–MS instrument at Focus Technology Co. Ltd, Nanjing, China. Instrument operating conditions and the data reduction method have been described by Hou et al. (2009) and Gao et al. (2013). Helium was used as a carrier gas and argon as a makeup gas. Analyses involved a laser spot diameter of 40 μm, 10 Hz ablation frequency, 20 s background data acquisition, and 40 s sample data acquisition. Elemental contents were calibrated against multiple reference materials (GSE-1G, BCR-2G, and BIR-1G), with ^{57}Fe used as the internal standard (Gao et al., 2013). The standards were analyzed after every 10 samples to correct for time-dependent instrumental drift and mass discrimination. Offline data reduction was performed using ICPMS DataCal software (Liu et al., 2008) and included selection of background and analytical signals, time drift corrections, and quantitative calibrations. Precision and accuracy were better than ±10%. Further details of the data reduction techniques are provided by Xie et al. (2008).

5. Results

5.1. Magnetic susceptibility of granitoids in the Huangshaping deposit

Thirteen granite porphyry, 7 felsite, and 9 quartz porphyry samples

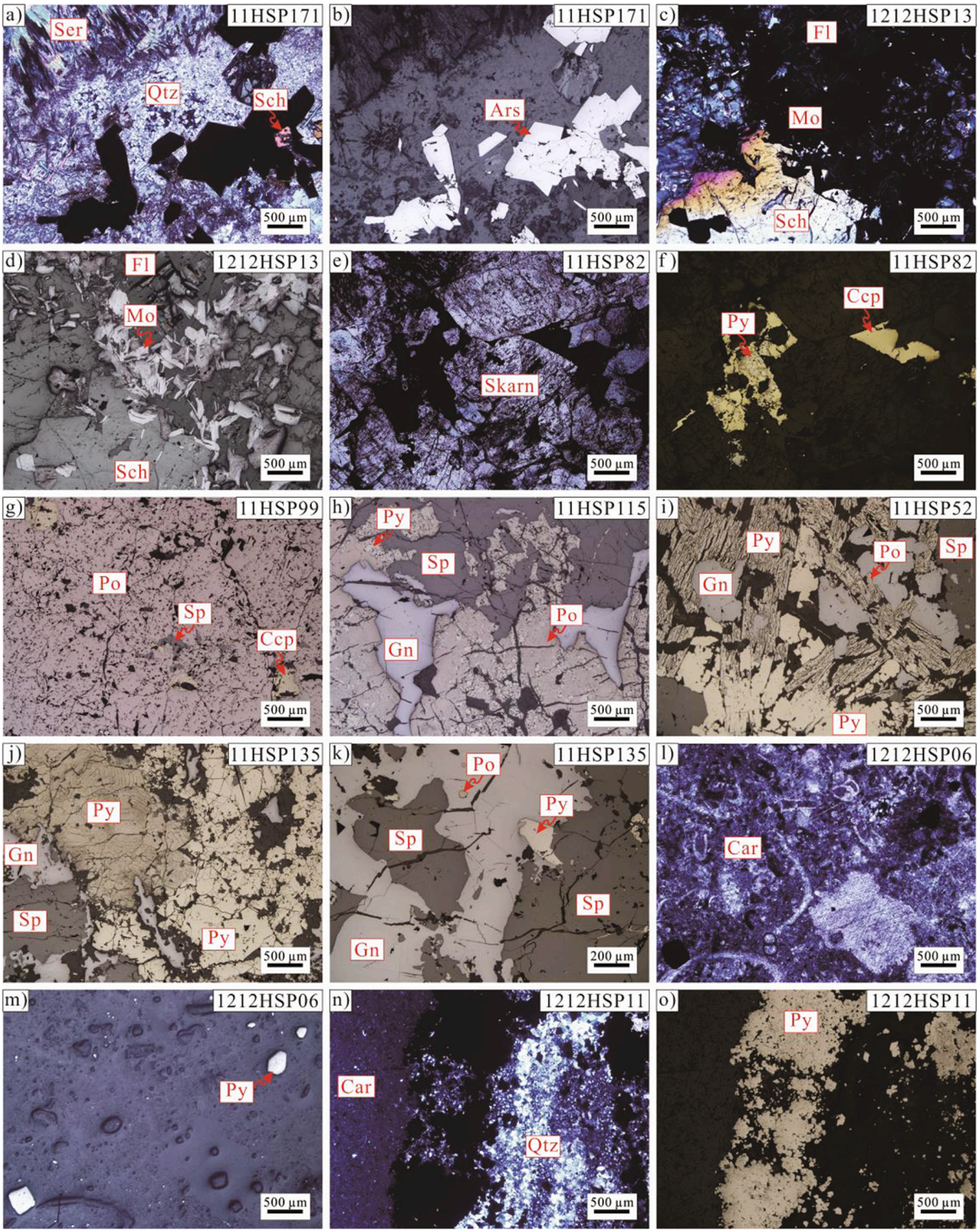

Fig. 5. Photomicrographs showing the occurrence of main sulfides in proximal skarn, the distal Pb–Zn orebody, and sedimentary carbonate in the Huangshaping deposit. (a, b) Euhedral arsenopyrite in a sericite–quartz alteration vein crosscutting granite porphyry (a, CPL; b, RL); (c, d) scheelite and molybdenite coexisting in a fluorite vein (c, CPL; d, RL); (e, f) chalcopyrite replacing pyrite, with both replacing skarn minerals or filling the space between them (e, CPL; f, RL); (g) massive pyrrhotite containing anhedral grains of chalcopyrite and sphalerite (RL); (h) pyrrhotite replaced by pyrite, sphalerite, and galena; sphalerite replaced by galena (RL); (i) pyrite replacing pyrrhotite, retaining the pseudomorphic textures of pyrrhotite; galena fills the space between these pyrite grains (RL); (j) colloform pyrite surrounded by recrystallized pyrite (RL); (k) pyrite replaced by sphalerite and galena; sphalerite replaced by galena, with pyrrhotite relicts contained in galena (RL); (l, m) euhedral pyrite disseminated in sedimentary carbonate containing abundant macrofossils (l, CPL; m, RL); (n, o) pyrite vein with quartz crosscutting sedimentary carbonate (n, CPL; o, RL). Ser, sericite; Ars, arsenopyrite; Car, carbonate; other abbreviations as in Fig. 4.

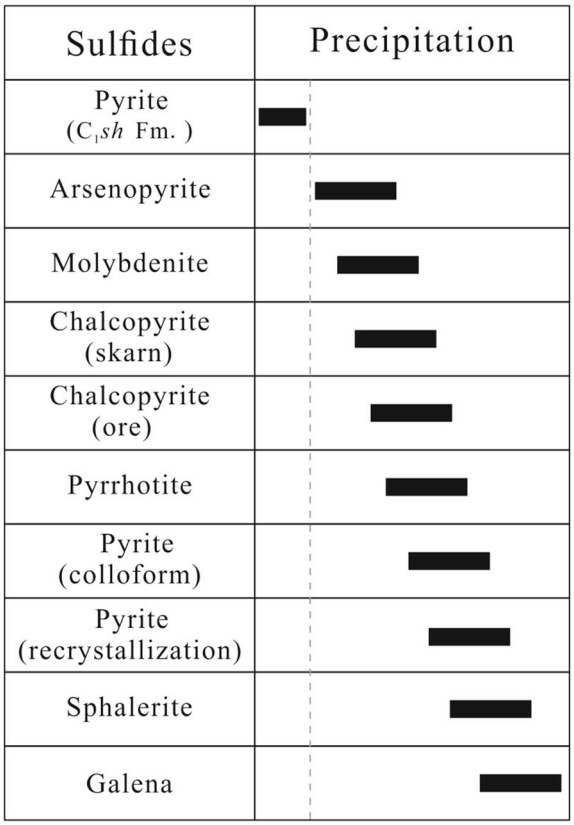

Fig. 6. Paragenetic sequence of the major sulfides in the Huangshaping deposit.

from the Huangshaping deposit, and 13 granodiorite porphyry samples from the adjacent Baoshan Cu–Pb–Zn deposit were analyzed for magnetic susceptibility. The granite porphyry, felsite, and quartz porphyry have low and wide-ranging magnetic susceptibility (CGS) values of (0.33–57.86), (0.54–71.28), and (0.99–54.25) $\times$ 10^{-6} emu g^{-1}, respectively (Supplementary Table 1). The granodiorite porphyry has high MS values of (226.13–1540.70) $\times$ 10^{-6} emu g^{-1} (Supplementary Table 1). In the magnetite–ilmenite classification diagram (Fig. 7), all samples from the Huangshaping and Baoshan deposits plot in the ilmenite- and magnetite-series fields, respectively.

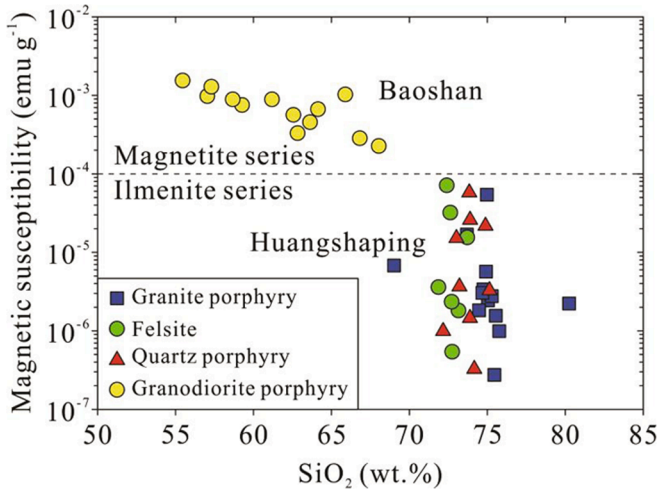

Fig. 7. Magnetic susceptibility vs. SiO_2 content for quartz porphyry, felsite, and granite porphyry of Huangshaping deposit, and granodiorite porphyry of the Baoshan deposit. Sampling locations and SiO_2 contents for the Huangshaping and Baoshan deposits are from Ding et al. (2016c) and Xie et al. (2013), respectively.

5.2. Trace element compositions

5.2.1. Pyrite

Results of trace element analyses are summarized in Supplementary Table 2 and illustrated in Fig. 8. On the basis of textures and paragenesis, three types of pyrite from the Huangshaping deposit were analyzed for their major and trace element compositions: pyrite disseminated in lower Carboniferous Shidengzi Formation limestone (Py(C_1sh)), pyrite with colloform texture (Py(c)), and pyrite that had undergone recrystallization (Py(r)). The pyrites have compositions of: S, 455,073–574,043 ppm; Fe, 416,918–535,497 ppm; Cu, below detection (b.d.)–937 ppm); Pb, 0.49–22,511 ppm; Zn b.d.–792 ppm; Se, b.d.–6.84 ppm; Te, b.d.–10.3 ppm; Co, b.d.–18.4 ppm; Ni, b.d.–624 ppm; Mn, b.d.–3984 ppm; Cd, b.d.–1.77 ppm; In, b.d.–4.06 ppm; Sn, b.d.–940 ppm; Bi, b.d.–4.44 ppm; As, b.d.–678 ppm; Sb, b.d.–3739 ppm; Mo, b.d.–75.6 ppm; Ag, b.d.–1863 ppm; Au, b.d.–0.97 ppm. Py(c) generally has higher contents of most elements than Py(r) and Py(C_1sh), except Se, Te, Co, and Ni. Te contents are comparable in the three types of pyrite. Py(C_1sh) has higher Se (1.48–6.04 ppm), Co (0.01–18.4 ppm), and Ni (0.99–624 ppm) contents than the other types, and the lowest Zn (b.d.–11.1 ppm), In (b.d.), Sn (b.d.–0.37), Sb (b.d.–0.38 ppm), and Ag (b.d.–0.01 ppm) contents.

5.2.2. Sphalerite

Sphalerites from the granodioritic enclaves (Sp(e)) and sulfide ores (Sp(o)) of the Huangshaping deposit have the following trace element compositions: S, 256,683–311,750 ppm; Zn, 571,613–628,023 ppm; Fe, 94,015–118,750 ppm; Cu, 729–10,104 ppm; Pb, 1.41–4194 ppm; Se, 0.85–12.3 ppm; Te, b.d.–0.69 ppm; Co, 0.17–270 ppm; Ni, b.d.–2.58 ppm; Mn, 896–2320 ppm; Cd, 1200–2117 ppm; In, 12.4–268 ppm; Sn, 1.69–123 ppm; Bi, b.d.–158 ppm; As, b.d.–5.62 ppm; Sb, 0.02–10.0 ppm; Mo, b.d.–0.15 ppm; Ag, 5.22–182 ppm; Au, b.d.–0.62 ppm. Sp(e) generally has higher Se, Te, Co, Ni, Mn, In, and Bi contents; Sp(e) and Sp(o) have comparable Fe, Cu, Sn, and Au contents; Sp(o) has higher Pb, Cd, As, Sb, Mo, and Ag contents.

5.2.3. Pyrrhotite

Pyrrhotites from the granodioritic enclaves (Po(e)) and sulfide ores (Po(o)) of the Huangshaping deposit have the following trace element compositions: S, 382,820–495,484 ppm; Fe, 499,260–616,733 ppm; Cu, b.d.–12,172 ppm; Pb, 0.13–220 ppm; Zn, b.d–24,114 ppm; Se, 0.73–19.5 ppm; Te, b.d.–7.84 ppm; Co, 0.93–635 ppm; Ni, 28.4–218 ppm; Mn, b.d.–21.4 ppm; Cd, b.d.–59.2 ppm; In, b.d.–133 ppm; Sn, b.d.–828 ppm; Bi, 0.05–56.2 ppm; As, b.d.–29.6 ppm; Sb, b.d.–4.59 ppm; Mo, b.d.–1.80 ppm; Ag, 0.21–39.1 ppm; Au, b.d.–0.06 ppm. Po(e) generally has higher contents of most of these elements, except Fe, As, and Mo; Po(e) and Po(o) Fe and As contents are comparable, and Po(e) Mo contents lower.

5.2.4. Chalcopyrite

Three types of chalcopyrite in enclaves (Ccp(e)), skarn (Ccp(s)), and sulfide ores (Ccp(o)) from the Huangshaping deposit have the following trace element compositions: S, 305,439–452,974 ppm; Cu, 148,917–370,352 ppm; Fe, 256,312–411,133; Pb, 1.24–62.3 ppm; Zn, 1408–35,437 ppm; Se, 1.86–17.1 ppm; Te, b.d.–22.7 ppm; Co, b.d.–275 ppm; Ni, 0.18–83.1 ppm; Mn, b.d.–108 ppm; Cd, 2.80–76.6 ppm; In, 1.81–218 ppm; Sn, 31.6–3634 ppm; Bi, 0.73–142 ppm; As, 6.22–32.1 ppm; Sb, b.d.–5.08 ppm; Mo, b.d.–1.59 ppm; Ag, 1.39–308 ppm; Au, b.d.–0.44 ppm. The three chalcopyrites have comparable Fe, Cu, Zn, Ni, Mn, Bi, and As contents; Ccp(e) has higher Te, Co, Ag, and Au contents; Ccp(s) has the lowest Pb, Sb, and Mo, but highest Cd, In, and Sn contents; Ccp(o) has the lowest Se, Co, In, and Au contents.

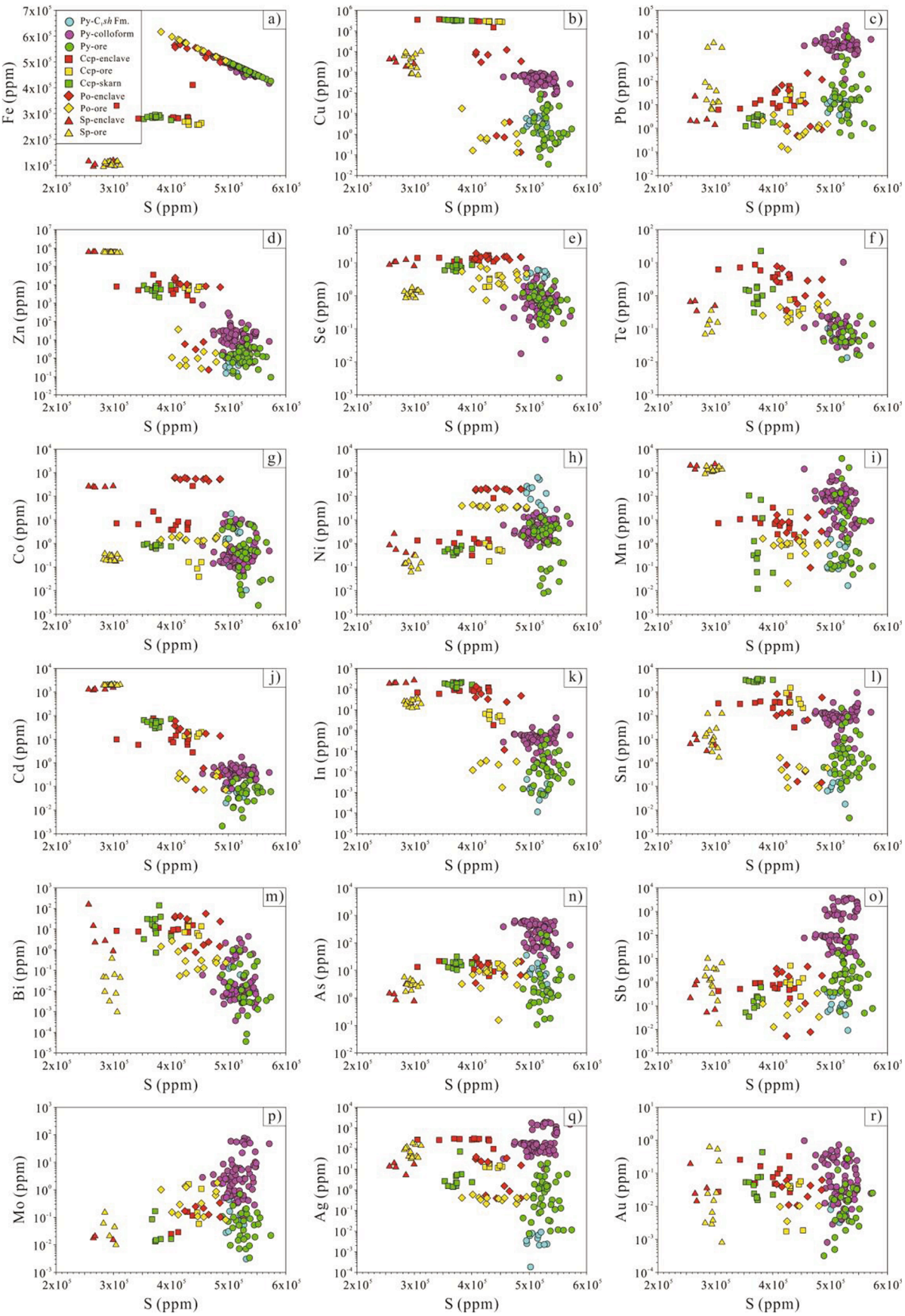

Fig. 8. Elemental compositions vs. S contents for sulfides of the Huangshaping deposit. (a) Fe; (b) Cu; (c) Pb; (d) Zn; (e) Se; (f) Te; (g) Co; (h) Ni; (i) Mn; (j) Cd; (k) In; (l) Sn; (m) Bi; (n) As; (o) Sb; (p) Mo; (q) Ag; (r) Au.

6. Discussion

6.1. Evolution of the Pb–Zn-bearing fluids: Insights from pyrite compositions

Pyrite (FeS_2) is the most abundant and widespread sulfide mineral in Earth's crust, occurring in settings as diverse as sediments, igneous rocks, hydrothermal deposits, and metamorphic terranes (e.g., Craig et al., 1998; Large et al., 2009, 2011, 2014). Trace elements are likely incorporated into pyrite as stoichiometric substitutions (e.g., Co, Ni, Se, and Te), non-stoichiometric substitutions (e.g., As, Mo, Au, and Tl), and as mineral inclusions (e.g., Cu, Pb, and Zn) (Huston et al., 1995; Large et al., 2007; Gregory et al., 2015). Elements with similar characteristics may enter sulfides in similar ways, but their elemental ratios may vary because their incorporation can be substantially affected by the physicochemical conditions of ore-forming fluids, such as temperature, pH, redox state, and ligands involved (e.g., Von Damm, 1990; Seyfried and Ding, 1993, 1995; Pokrovski et al., 2008; Keith et al., 2016; Hannah et al., 2018). Elemental ratios in pyrite, particularly S/Se, Se/Te, and Co/Ni, can therefore be used as indicators that reflect the temperatures and sources of hydrothermal fluids where the pyrite precipitated. Previous studies have shown that volcanogenic pyrite, or pyrite precipitated from magmatic–hydrothermal fluids, has elevated Co contents (Cafagna and Jugo, 2016; Shao et al., 2018), whereas sedimentary pyrite, such as that in black shale, has high Ni contents (Large et al., 2009; Gregory et al., 2015). Furthermore, Co usually prefers to enter pyrite at high temperatures during recrystallization and metamorphism (Conn, 2019). Consequently, Co/Ni ratios of <1 (with low standard deviations) are commonly accepted as indicating pyrite of sedimentary origin, while pyrite associated with hydrothermal fluids has Co/Ni ratios of ≫1 (e.g., Bralia et al., 1979; Raymond, 1996; Koglin et al., 2010; Thomas et al., 2011; Deol et al., 2012; Zhang et al., 2014; Meng et al., 2019; Mukherjee et al., 2019).

Pyrite in sulfide ores of the Huangshaping deposit, including early Py (c), late Py(r), and Py(C_1sh) is disseminated within strata. Py(c) generally has much higher contents of most trace elements than Py(r), but with comparable contents of Se, Te, Co, Ni, and Bi (Fig. 8), due mainly to the expulsion of trace elements during recrystallization. Previous studies have shown that recrystallization of pyrite results in the expulsion of most trace elements bound loosely in the pyrite structure as non-stoichiometric substitutions and mineral inclusions (e.g., Cu, Pb, Zn, Bi, Mo, Ag, and Au); stoichiometric substitutions (e.g., Co, Ni, Se, and Te) are incorporated tightly into the structure, allowing the primary contents of these elements to be retained (Huston et al., 1993, 1995; Large et al., 2007; Genna and Gaboury, 2015). Bismuth can substitute into pyrite together with Ag, Pb, and Sb (Huston et al., 1995), meaning that the comparable concentrations of Bi in Py(r) and Py(c) are due mainly to substitution of Ag by Bi during recrystallization. Despite the expulsion of elements during pyrite recrystallization, Py(r) and Py(c) have similar Co/Ni ratios, distinct from those of Py(C_1sh) (Fig. 9a). This means that the physicochemical conditions of ore-forming fluids may not have significantly changed from precipitation of Py(c) to Py(r). The relatively high Co/Ni ratios in Py(c) and Py(r), compared to Py(C_1sh), indicate that pyrite in the ores precipitated from relatively high-temperature fluids significantly influenced by magmatic–hydrothermal fluids.

In addition to similar Co/Ni ratios, Py(r) and Py(c) also have similar Zn/Cd, Cu/In, and Pb/Sb ratios (Fig. 9b–d). Cadmium can substitute for Zn in sphalerite, suggesting that submicroscopic sphalerite inclusions likely account for most Zn and Cd in other sulfides, such as pyrite, chalcopyrite, and galena (Cook et al., 2009; Belissont et al., 2014; Zhu et al., 2016, 2018). Similarly, high Sn and In contents in pyrite may be

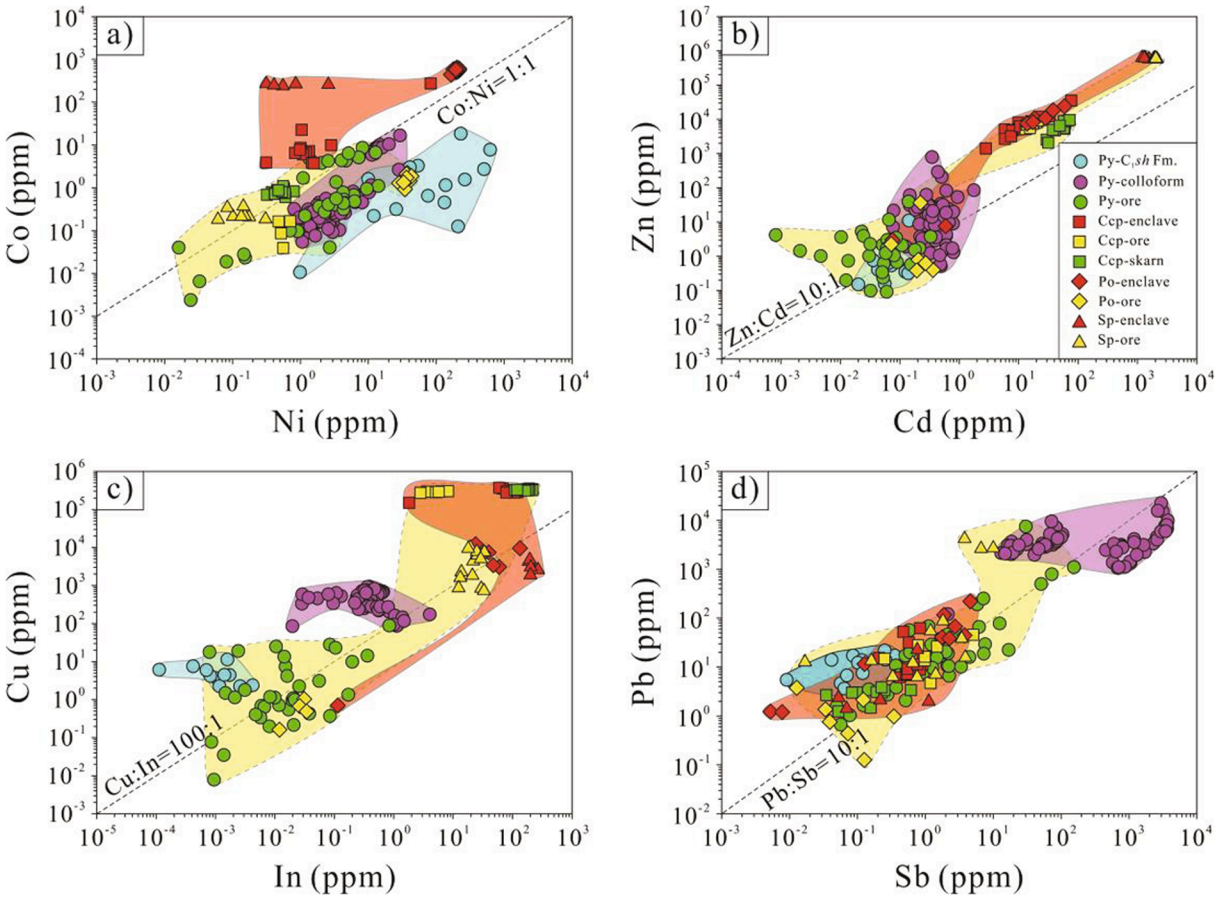

Fig. 9. Bivariate graphs showing the relationships between trace element contents. (a) Co–Ni; (b) Zn–Cd; (c) Cu–In; (d) Pb–Sb.

due to inclusions of chalcopyrite, as these elements can substitute into the Fe site of chalcopyrite, forming crystals that are isostructural with chalcopyrite, such as roquesite ($CuInS_2$) and stannite (Cu_2FeSnS_4) (Huston et al., 1995). Moreover, Sb, Pb, and Ag can occur in pyrite as inclusions enriched in Sb, Pb, and Ag, such as in argentiferous tetrahedrite ($(Cu, Fe)_{12}Sb_4S_{13}$) (Huston et al., 1995), resulting in Ag and Sb commonly entering sulfides by substitution for other elements. Regarding pyrite paragenesis, Py(c) precipitated first, before being significantly refined by late sphalerite- and galena-bearing fluids, forming Py(r). Despite the general evolution of ore-bearing fluids, the similar ratios of Co/Ni, Zn/Cd, Cu/In, and Pb/Sb in Py(r) and Py(c) indicate that the hydrothermal fluids from which they precipitated were not significantly different.

6.2. *Possible contributions of basement: Insights from sulfides in granodioritic enclaves*

Granodioritic enclaves in the quartz porphyry contain abundant sulfides, including chalcopyrite, sphalerite, and pyrrhotite (Fig. 4), with sulfide assemblages of relatively high temperature and low sulfur fugacity. Although questions remain concerning the behavior of trace elements in pyrrhotite, the major elements in this sulfide are S and Fe, similar to pyrite, indicating that trace elements may have similar behaviors when substituted into pyrrhotite and pyrite. The Po(e) generally has higher concentrations of most trace elements than Po(o) (Fig. 8), which indicates that the Po(e) precipitated in high-temperature hydrothermal fluids significantly influenced by magmatic fluids, leading to high solubility for most of these trace elements (Keith et al., 2016; Hannah et al., 2018). This is further confirmed by Po(e) having much higher Co/Ni ratios than those of Po(o) (Fig. 9a). Although it is still unclear how Co and Ni substitute in sphalerite and chalcopyrite, they are likely incorporated by substituting for Fe, as these elements have similar behaviors in sulfides. This may explain why Sp(e) and Ccp(e) also have higher Co/Ni ratios than those in Sp(o) and Ccp(o) (Fig. 9a). Consequently, sulfides in granitic enclaves (Po(e), Sp(e), and Ccp(e)) have much higher Co/Ni ratios than those in distal sulfide ores (Po(o), Sp(o), and Ccp(o)), indicating that the sulfides in the granodioritic enclaves likely precipitated in high-temperature hydrothermal fluids significantly influenced by magmatic–hydrothermal fluids. Ccp(s) has Co/Ni ratios between those of Ccp(e) and Ccp(o), mainly because this mineral precipitated in skarn formed between granitoids and distal sulfide ores. This further suggests that, in addition to pyrite, the Co/Ni ratios of other sulfides can also effectively reflect the fluid environments from which they precipitated.

Submicroscopic sphalerite and chalcopyrite inclusions likely account for most Zn, Cd, Sn, and In in other sulfides. Unlike the Co/Ni ratio, which is predominantly controlled by temperature and magmatic fluids, sulfides in granodioritic enclaves (Po(e), Sp(e), and Ccp(e)) have similar Zn/Cd, Cu/In, and Pb/Sb ratios to those in the ores (Po(o), Sp(o), Ccp(o), Py(c), and Py(r)) (Fig. 9b–d). This means that the metal sources for sulfides in the granodioritic enclaves and ores are likely the same. For ore-forming metals Cu and Zn, sulfides in the enclaves generally have high contents, mainly because of the high temperatures of the hydrothermal fluids from which they precipitated. However, sulfides in enclaves and most sulfides in ores have relatively low Pb contents, significantly lower than those of Py(c) (Fig. 9d), likely because Pb is rejected by these sulfides at higher temperatures and expelled from the sulfide structures, forming galena at low temperatures. This may also explain the lack of galena in the enclaves (Fig. 4). However, the high Pb and Sb contents of Py(c) suggest that the ore-forming fluids were initially enriched in ore-forming Pb. Therefore, based on the Co/Ni, Zn/Cd, Cu/In, and Pb/Sb ratios of sulfides, we propose that the sulfides in both enclaves and ores were precipitated from hydrothermal fluids derived from the same single source, although the temperature was higher for sulfides precipitated in the enclaves. This conclusion is consistent with published Pb isotopic compositions of sulfides in the Huangshaping deposit, which exhibit positive correlations between ^{206}Pb, ^{207}Pb, and ^{208}Pb, and plot in the field for metamorphic rocks beneath the deposit, suggesting that leaching of metals from the basement dominated the formation of Pb–Zn mineralization (Ding et al., 2016b).

The abundant sulfides in the granodioritic enclaves indicate the input of sulfide-bearing magmas to the quartz porphyry in the Huangshaping deposit. On the basis of the geochemical compositions of zircon and apatite in the enclaves, a previous study proposed that these enclaves are compositionally similar to the Pb–Zn-bearing granodiorite porphyries in southern Hunan Province, but distinct from that of the host-rock quartz porphyry, felsite, and granite porphyry in this deposit (Ding et al., 2016c). The Pb–Zn-bearing granodiorite porphyries in southern Hunan Province, such as in the Baoshan (Xie et al., 2013), Shuikoushan (Zuo et al., 2014), and Tongshanling (Huang et al., 2017) deposits, were generally considered to have resulted from the melting of mafic *meta*-igneous rocks within the lower crust, including mafic granulitic and/or amphibolitic basement (Huang et al., 2017). This suggests that granodioritic activity must have occurred due to the melting of lower crust before, or coeval with, the intrusion of quartz porphyry in the Huangshaping deposit. Economic Pb–Zn mineralization in southern Hunan Province is closely associated with the granodiorite porphyries, and their relatively high Cl contents and oxygen fugacity are considered crucial for sulfide mineralization (Ding et al., 2015), which can effectively accumulate and transport chalcophile elements (e.g., Cu, Pb, and Zn) in magmatic and hydrothermal systems (Sun et al., 2004, 2013; Nadeau et al., 2010). The granodioritic activity beneath the Huangshaping deposit is therefore most likely to have caused significant accumulation of Pb and Zn in the metamorphic or crystalline basement beneath the deposit, with the Pb–Zn-bearing basement being the source of late Pb–Zn mineralization in the Huangshaping deposit.

6.3. *Possible model for distal Pb–Zn mineralization in the Huangshaping deposit*

Sulfide mineralization associated with granodioritic activity beneath the Huangshaping deposit may have contributed to Pb–Zn mineralization in the deposit in several ways, including: (1) the addition of sulfide-bearing basement material to the magma by re-melting or contamination, with this mingling causing the formation of sulfide-bearing magma (quartz porphyry) and later the orebodies; (2) the provision of heat by granitoids in the Huangshaping deposit (but no sulfur, fluids, or metals) with the heat driving hydrothermal circulation that leached metals from the Pb–Zn-bearing basement (Vikre et al., 2011; Gigon et al., 2020). A previous study has shown that the quartz porphyry, felsite, and granite porphyry are more depleted in radiogenic Pb than sulfides in ores, meaning that these granitoids were not the primary metal source for sulfide ores in this deposit (Ding et al., 2016b). Granitoid magnetic susceptibility is sensitive to their redox state and an effective means of distinguishing oxidized magnetite-series from reduced ilmenite-series granitoids (Ishihara, 1977, 1981). Granitoids in the Huangshaping deposit have low CGS values indicating they are reduced ilmenite-series rocks, while Pb–Zn-bearing granodiorite porphyry of the Baoshan deposit is of the oxidized magnetite-series (Fig. 7). This conclusion is in consistent with the fact that the magnetite is rare in the granitoids from the Huangshaping deposit (Fig. 4), but it is abundant in the granodiorite porphyry from the Baoshan deposit (Xie et al., 2013). The reduced state of the Huangshaping granitoids suggests they were not available for the accumulation and migration of sulfide, significantly limiting their direct contribution of metals. This is distinct to the Baoshan deposit, which is one of the typical skarn Pb–Zn deposits in this southern Hunan Province with pyrite, sphalerite, and galena as the major distal sulfides as well as the Huangshaping deposit. The metals in the Baoshan deposit most likely directly dominated by the oxidized granodiorite porphyry as the metals can be accumulated and transported more effectively in oxidized systems (Ding et al., 2015), this conclusion is further evidenced by that

the granodiorite porphyry and the sulfides from this deposit have similar Pb isotopic compositions (Xie et al., 2015; Ding et al., 2016a).

The formation of the Huangshaping deposit may therefore have involved processes similar to (2) above. The leaching of metals, such as Pb and Zn, by fluid flow during regional metamorphism or from crystalline basement material is considered one of the most important processes involved in the formation of giant Pb–Zn deposits associated with hydrothermal activity (Haack et al., 1984; Townley and Godwin, 2001; Oliver et al., 2006; Cunha et al., 2007). Pb and Zn losses associated with such leaching in high-grade metamorphic zones have been calculated to reach values of 2.7 and 27 Mt, respectively (Hammerli et al., 2015a, 2015b). Granite porphyry, which ascended and crystallized more slowly than the other two granitoids (as indicated by its porphyritic texture), is not enriched in Cl, similar to the other W–Sn-bearing granites in southern Hunan Province. However, this rock has much higher F contents (3.15–4.53 wt% F in the biotite) than those of the other W–Sn-bearing granites (0.04–3.97 wt%) (Ding et al., 2015, 2017). Fluorine can dramatically reduce the solidus temperature of granitic melts (Minning, 1981; Webster et al., 1987), meaning that the exsolution of magmatic fluids can be sustained for long periods (Chang and Meinert, 2008). Magmatic sulfides can be concentrated within the batholith and finally transported by hydrothermal fluids exsolved from the magma, forming giant porphyry–epithermal sulfide deposits (Halter et al., 2002, 2005; Nadeau et al., 2010; Wilkinson, 2013; Mungall et al., 2015; Bai et al., 2020). Granitoids in the Huangshaping deposit, especially granite porphyry, could therefore have provided large amounts of heat and fluids, both of which are fundamental to hydrothermal activity and the extraction of metals from basement material. This is consistent with the $\delta^{34}S$ values of sulfides increasing outward from the granite porphyry (Zhu et al., 2012).

In southern Hunan Province, Pb–Zn-bearing granodiorite porphyries (*ca.* 160 Ma) intruded ~ 5 Myr before the W–Sn-bearing granites (*ca.* 155 Ma). This time gap is considered to represent the melting sequence of lower (mainly *meta*-mafic) and upper (mainly *meta*-sedimentary) crust triggered by the underplating of basaltic magmas (e.g., Ding et al., 2015; Huang et al., 2017). Similarly, in the Huangshaping deposit, quartz porphyry and granitic enclaves (*ca.* 160 Ma) also intruded ~ 5 Myr earlier than felsite and granite porphyry (*ca.* 155 Ma) (Ding et al., 2016c). Therefore, the coexistence of economic W–Mo and Pb–Zn mineralization in this deposit was likely controlled by the overlap of early granodioritic and late granitic magmatism. The W–Mo mineralization was closely associated with the granite porphyry, which displays features of the melting of *meta*-sedimentary basement in the upper crust (Yao et al., 2005; Li et al., 2014a; Ding et al., 2016c). Although granodiorite porphyry has not been observed in the Huangshaping deposit, the granodioritic enclaves indicate such rocks exist beneath it, which may have been associated with the accumulation of the ore-forming metals Pb and Zn in the upper crustal basement. The subsequent intrusion of granitoids leached these metals from the upper crust and transported them towards the surface, precipitating as distal Pb–Zn mineralization, as summarized in Fig. 10.

7. Conclusions

(1) The Huangshaping deposit is unique for the coexistence of economic W–Mo and Pb–Zn mineralization associated with reduced granitoids, including quartz porphyry, felsite, and granite porphyry. Granodioritic enclaves occur in the quartz porphyry and contain abundant sulfides including chalcopyrite, sphalerite, and pyrrhotite.

(2) The sulfides from the granodioritic enclaves have higher Co/Ni ratios than those of the distal Pb–Zn ores, but similar Zn/Cd, Cu/In, and Pb/Sb ratios, indicating that sulfides in both enclaves and ores were precipitated from hydrothermal fluids derived from the same single source, although the temperature was higher when they precipitated in the enclaves.

(3) Granodioritic intrusive activity that occurred ~5 Myr before the granitoids in the Huangshaping deposit resulted in significant accumulation of metals in metamorphic or crystalline basement. The metals in the basement were scavenged by hydrothermal circulation triggered by late intrusions of felsite and granite porphyry, especially by fluorine-rich granite porphyry, forming the distal Pb–Zn mineralization near the surface of the deposit. The accumulation of sulfides triggered by earlier granodioritic activity was crucial for the formation of the distal sulfide mineralization in the Huangshaping deposit, and probably also important for that in the other W–Mo deposits related to reduced granites in southern Hunan Province.

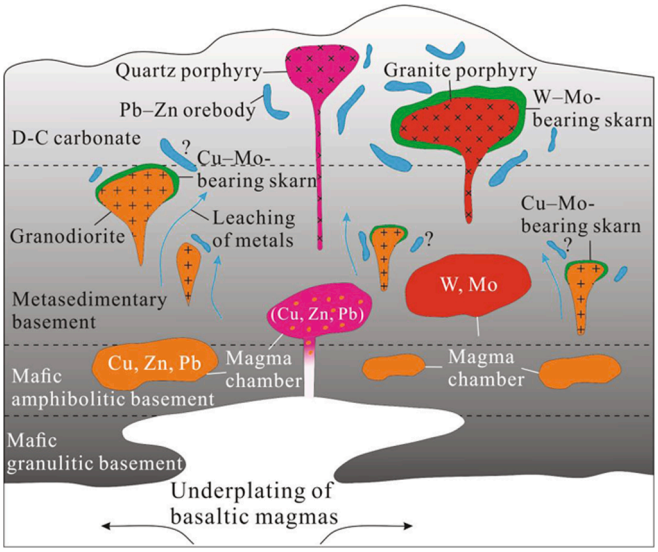

Fig. 10. Model showing the relationship between intrusion of igneous rocks and the formation of Pb–Zn mineralization in the Huangshaping deposit. The possible basement types are modified after Huang et al. (2017). For more details see Section 6.3.

Declaration of Competing Interest

The authors declare that they have no known competing financial interests or personal relationships that could have appeared to influence the work reported in this paper.

Acknowledgements

We are grateful to Dr. Huan Li, an anonymous reviewer, Dr. Lebing Fu (Editor) and Dr. Franco Pirajno (Editor-in-Chief) for their thoughtful reviews and constructive comments. This research was financially supported by the Foundation for Young Scientists of Jiangsu Province (Grant BK20180511), Key Laboratory of Ocean and Marginal Sea Geology, Chinese Academy of Sciences (Grant OMG2019-07), Scientific Research Fund of the Second Institute of Oceanography, MNR (Grand JB2001), National 305 Project of China (Grant 2019B00011-1), National Science Foundation for Young Scientists of China (Grants 41803037 and 41806076), China Postdoctoral Science Foundation (Grant 2019M652043), Open Research Fund Program of State Key Laboratory for Mineral Deposits Research, Nanjing University (Grant 2020-LAMD-K05), and Open Research Fund Program of Key Laboratory of Metallogenic Prediction of Nonferrous Metals and Geological Environment Monitoring (Central South University), Ministry of Education (Grant 2019YSJS03).

Appendix A. Supplementary data

Supplementary data to this article can be found online at https://doi.org/10.1016/j.oregeorev.2020.103939.

References

Akiska, S., Demirela, G., Sayili, S.I., 2013. Geology, mineralogy and the Pb, S isotope study of the Kalkım Pb–Zn ± Cu deposits, Biga Peninsula, NW Turkey. J. Geosci. 58, 379–396.

Ault, K.M., Williams-Jones, A.E., 2004. Sulfur and lead isotope study of the El Mochito Zn–Pb–Ag deposit. Econ. Geol. 99, 1223–1231.

Bai, Z.J., Zhong, H., Hu, R.Z., Zhu, W.G., 2020. Early sulfide saturation in arc volcanic rocks of southeast China: implications for the formation of co-magmatic porphyry–epithermal Cu–Au deposits. Geochim. Cosmochim. Acta. https://doi.org/10.1016/j.gca.2020.04.014.

Belissont, R., Boiron, M.C., Luais, B., Cathelineau, M., 2014. LA-ICP-MS analysis of minor and trace elements and bulk Ge isotopes in zoned Ge-rich sphalerited from the NOailhac-Saint-Salvy deposit (France): insights into incorporation mechanisms and ore deposition process. Geochim. Cosmochim. Acta 126, 518–540.

Bralia, A., Sabatini, G., Troja, F., 1979. A revaluation of the Co/Ni ratio in pyrite as geochemical tool in ore genesis problems. Miner Deposita 14, 353–374.

Cafagna, F., Jugo, P.J., 2016. An experimental study on the geochemical behavior of highly siderophile elements (HSE) and metalloids (As, Se, Sb, Te, Bi) in a mss-iss-pyrite System at 650 °C: A possible magmatic origin for Co-HSE-bearing pyrite and the role of metalloid-rich phases in the fractionation of HSE. Geochim. Cosmochim. Acta. https://doi.org/10.1016/j.gca.2015.12.035.

Chang, Z.S., Meinert, L.D., 2008. The Empire Cu–Zn mine, Idaho: Exploration implications of unusual skarn features related to high fluorine activity. Econ. Geol. 103, 909–938.

Conn, C.D., 2019. The effects of amphibolite facies metamorphism on the trace element composition of pyrite and pyrrhotite in the Cambrian Nairne Pyrite Member, Kanmantoo Group, South Australia. Graduate Theses and Dissertations. Iowa State University. P212.

Cook, N.J., Ciobanu, C.L., Pring, A., Skinner, W., Shimizu, M., Danyushevsky, L., Saini-Eidukat, B., Melcher, F., 2009. Trace and minor elements in sphalerite: a LA-ICPMS study. Geochim. Cosmochim. Acta 73, 4761–4791.

Craig, J.R., Vokes, F.M., Solberg, T.N., 1998. Pyrite: physical and chemical textures. Miner. Deposita 34, 82–101.

Cunha, I.A., Misi, A., Babinski, M., Iyer, S.S.S., 2007. Lead isotope constraints on the genesis of Pb–Zn deposits in the Neoproterozoic Vazante Group, Minas Gerais, Brazil. Gondwana Res. 11, 382–395.

Deol, S., Deb, M., Large, R.R., Gilbert, S., 2012. LA-ICPMS and EPMA studies of pyrite, arsenopyrite and loellingite from the Bhukia-Jagpura gold prospect, southern Rajasthan, India: Implications for ore genesis and gold remobilization. Chem. Geol. 326–327, 72–87.

Ding, T., Ma, D.S., Lu, J.J., Zhang, R.Q., 2015. Apatite in granitoids related to polymetallic mineral deposits in southeastern Hunan Province, Shi-Hang zone, China: Implications for petrogenesis and metallogenesis. Ore Geol. Rev. 69, 104–117.

Ding, T., Ma, D.S., Lu, J.J., Zhang, R.Q., 2018a. Garnet and scheelite as indicators of multi-stage tungsten mineralization in the Huangshaping deposit, southern Hunan province, China. Ore Geol. Rev. 94, 193–211.

Ding, T., Ma, D.S., Lu, J.J., Zhang, R.Q., 2018b. Magnetite as an indicator of mixed sources for W-Mo-Pb-Zn mineralization in the Huangshaping polymetallic deposit, southern Hunan Province, China. Ore Geol. Rev. 95, 65–78.

Ding, T., Ma, D.S., Lu, J.J., Zhang, R.Q., Zhang, S.T., 2017. Mineral geochemistry of granite porphyry in Huangshaping pollymetallic deposit, southern Hunan Province, and its implications for metallogensis of skarn scheelite mineralization. Acta Petrol. Sin. 33, 716–728 (in Chinese with English abstract).

Ding, T., Ma, D.S., Lu, J.J., Zhang, R.Q., Xie, Y.C., 2016a. Sulfur and lead isotopic compositions of granitoids and fluid inclusions in Baoshan deposit, Hunan Province. Mineral Deposit 35 (4), 663–676 (in Chinese with English abstract).

Ding, T., Ma, D.S., Lu, J.J., Zhang, R.Q., Zhang, S.T., 2016b. S, Pb, and Sr isotope geochemistry and genesis of Pb–Zn mineralization in the Huangshaping polymetallic ore deposit of southern Hunan Province, China. Ore Geol. Rev. 77, 117–132.

Ding, T., Ma, D.S., Lu, J.J., Zhang, R.Q., Zhang, S.T., Gao, S.Y., 2016c. Petrogenesis of Late Jurassic granitoids and relationship to polymetallic deposits in southern China: The Huangshaping example. Int. Geol. Rev. 58, 1646–1672 (in Chinese with English abstract).

Gao, J.F., Zhou, M.F., Lightfoot, P.C., Wang, C.Y., Qi, L., Sun, M., 2013. Sulfide saturation and magma emplacement in the formation of the Permian Huangshandong Ni-Cu Sulfide Deposit, Xinjiang, Northwestern China. Econ. Geol. 108, 1833–1848.

Genna, D., Gaboury, D., 2015. Deciphering the hydrothermal evolution of a VMS system by LA-ICP-MS using trace elements in pyrite: An example from the Bracemac-McLeod deposits, Abitibi, Canada and implications for exploration. Econ. Geol. 110, 2087–2108.

Gigon, J., Deloule, E., Mercadier, J., Huston, D.L., Richard, A., Annesley, I.R., Wygralak, A.S., Skirrow, R.G., Mernagh, T.P., Masterman, K., 2020. Tracing metal sources for the giant McArthur River Zn-Pb deposit (Australia) using lead isotopes. Geology. https://doi.org/10.1130/G47001.1.

Gilder, S.A., Gill, J., Coe, R.S., Zao, X.X., Liu, Z.W., Wang, G.X., Yuan, K.R., Liu, W.L., Kuang, G.D., Wu, H.R., 1996. Isotopic and paleomagnetic constraints on the Mesozoic tectonic evolution of south China. J. Geophys. Res. 101, 16137–16154.

Gregory, D.D., Large, R.R., Halpin, J.A., Baturina, E.L., Lyons, T.W., Wu, S., Danyushevsky, L., Sack, P.J., Chappaz, A., Maslennikov, V.V., Bull.S.W.,, 2015. Trace element content of sedimentary pyrite in black shales. Econ. Geol. 110, 1389–1410.

Haack, U., Heinrichs, H., Boness, M., Schneider, A., 1984. Loss of metals from pelites during regional metamorphism. Contrib. Mineral Petrol. 85, 116–132.

Halter, W., Pettke, T., Heinrich, C., 2002. The origin of Cu/Au ratios in porphyry-type ore deposits. Science 296, 1844–1846.

Halter, W.E., Heinrich, C.A., Pettke, T., 2005. Magma evolution and the formation of porphyry Cu–Au ore fluids: evidence from silicate and sulfide melt inclusions. Miner Deposita 39, 845–863.

Hammerli, J., Spandler, C., Oliver, N.H.S., Sossi, P., Dipple, G.M., 2015a. Zn and Pb mobility during metamorphism of sedimentary rocks and potential implications for some base metal deposits. Miner Deposita 50 (6), 657–664. https://doi.org/10.1007/s00126-015-0600-5.

Hammerli, J., Spandler, C., Oliver, N.H.S., Sossi, P., Dipple, G.M., 2015b. Zn and Pb mobility during metamorphism of sedimentary rocks and potential implications for some base metal deposits. Miner Deposita. https://doi.org/10.1007/s00126-015-0600-5.

Hannah, L.J.G., Hannington, M.D., Petersen, S., Frische, M., Fuchs, S.H., 2018. Constraints on the behavior of trace elements in the actively-forming TAG deposit, Mid-Atlantic Ridge, based on LA-ICP-MS analyses of pyrite. Chem. Geol. https://doi.org/10.1016/j.chemgeo.2018.08.019.

Hou, K.J., Li, Y.H., Ye, T.R., 2009. In-situ U-Pb zircon dating laser ablation-multi iron counting-ICP-MS. Mineral Deposits 28, 481–492 (in Chinese with English abstract).

Hua, R.M., Zhang, W.L., Gu, S.Y., Chen, P.R., 2007. Comparison between REE granite and W-Sn granite in the Nanling region, south China, and their mineralizations. Acta Petrol. Sin. 23, 2321–2328 (in Chinese with English abstract).

Huang, C., Li, X.F., Wang, L.f., Liu, F.P., 2013. Fluid inclusion study of the Huangshaping polymetallic deposit, Hunan province, south China. Acta Petrol. Sin. 29 (12), 4232–4244 (in Chinese with English abstract).

Huang, X.D., Lu, J.J., Sizaret, S., Wang, R.C., Ma, D.S., Zhang, R.Q., Zhao, X., Wu, J.W., 2017. Petrogenetic differences between theMiddle-Late Jurassic Cu-Pb-Zn-bearing and W-bearing granites in the Nanling Range, South China: A case study of the Tongshanling and Weijia deposits in southern HunanProvince. Sci. Earth Sci. 60, 1220–1236.

Huang, X.D., Lu, J.J., Sizaret, S., Wang, R.C., Wu, J.W., Ma, D.S., 2018. Reworked restite enclave: Petrographic and mineralogicalconstraints from the Tongshanling intrusion, Nanling Range, South China. J. Asian Earth Sci. 166, 1–18.

Huston, D.L., Sie, S.H., Suter, G.F., Ryan, C.G., 1993. The composition of pyrite in volcanogenic massive sulfide deposits as determined by proton microprobe. Nucl. Instr. Meth. Phys. Res. B75, 531–534.

Huston, D.L., Sie, S.-H., Suter, G.F., Cooke, D.R., 1995. Trace Elements in Sulfide Minerals from Eastern Australian Volcanic-Hosted Massive Sulfide Deposits: Part I. Proton Microprobe Analyses of Pyrite, Chalcopyrite, and Sphalerite, and Part II. Selenium Levels in Pyrite: Comparison with δ34S Values and Implications for the Source of Sulfur in Volcanogenic Hydrothermal Systems. Econ. Geol. 90, 1167–1196.

Ishihara, S., 1977. The magnetite-series and ilmenite-series granitic rocks. Mining Geology 27, 293–305.

Ishihara, S., 1981. The granitoid series and mineralization. Economic Geology 75th anniversary volume, 458–484.

Jiang, W.C., Li, H., Li, H., Turner, S., Zhu, D.P., Wang, C., 2020. Timing and origin of multi-stage magmatism and related W-Mo–Pb–Zn–Fe–Cu mineralization in the Huangshaping deposit, South China: An integrated zircon study. Chem. Geol. 552, 119782.

Jiang, Y.H., Jiang, S.Y., Dai, B.Z., Liao, S.Y., Zhao, K.D., Ling, H.F., 2009. Middle to late Jurassic felsic and mafic magmatism in southern Hunan Province, southeast China: Implications for a continental arc to rifting. Lithos 107, 185–204.

Kalender, L., 2011. Oxygen, carbon and sulphur isotope studies in the Keban Pb–Zn deposits, eastern Turkey: An approach on the origin of hydrothermal fluids. J. Afr. Earth Sc. 59, 341–348.

Keith, M., Häckel, F., Haase, K.M., Schwarz-Schampera, U., Klemd, R., 2016. Trace element systematics of pyrite from submarine hydrothermal vents. Ore Geol. Rev. 72, 728–745.

Koglin, N., Frimmel, H.E., Minter, W.L., Brätz, H., 2010. Trace-element characteristics of different pyrite types in Mesoarchaean to Palaeoproterozoic placer deposits. Miner Deposita 45, 259–280.

Large, R.R., 1992. Australian volcanic-hosted massive sulfide deposits: Features, styles, and genetic models. Econ. Geol. 87, 471–510.

Large, R.R., Bull, S.W., Maslennikov, V.V., 2011. Carbonaceous sedimentary source-rock model for Carlin-type and orogenic gold deposits. Econ. Geol. 106, 331–358.

Large, R.R., Danyushevsky, L., Hollit, C., Maslennikov, V., Meffre, S., Gilbert, S., Bull, S., Scott, R., Emsbo, P., Thomas, H., Singh, B., Foster, J., 2009. Gold and trace element zonation in pyrite using a laser imaging technique: Implications for the timing of gold in orogenic and carlin-style sediment-hosted deposits. Econ. Geol. 104, 635–668.

Large, R.R., Halpin, J.A., Danyushevsky, L.V., Maslennikov, V.V., Bull, S.W., Long, J.A., Gregory, D.D., Lounejeva, E., Lyons, T.W., Sack, P.J., McGoldrick, P.J., Calver, C.R., 2014. Trace element content of sedimentary pyrite as a new proxy for deep-time ocean-atmosphere evolution. Earth Planet. Sci. Lett. 389, 209–220.

Large, R.R., Maslennikov, V.V., Robert, F., Danyushevsky, L.V., Chang, Z., 2007. Multistage sedimentary and metamorphic origin of pyrite and gold in the giant Sukhoi Log deposit, Lena gold province, Russia. Econ. Geol. 102, 1233–1267.

Lei, Z.H., Cen, F.W., Chen, Z.H., Xu, Y.M., Gong, S.Q., Li, H.Q., Mei, Y.P., Qu, W.J., Wang, D.H., 2010. Petrogenetic and metallogenic age determination of the Huangshaping lead–zinc polymetallic deposit and its geological significance. Acta Geosci. Sin. 31, 532–540 (in Chinese with English abstract).

Li, H., Palinkaš, L.A., Evans, N.J., Watanabe, K., 2020. Genesis of the Huangshaping W-Mo-Cu-Pb-Zn deposit, South China: Role of magmatic water, metasomatized fluids, and basinal brines during intra-continental extension. Geol. J. 55 (2), 1409–1430.

Li, H., Watanabe, K., Yonezu, K., 2014a. Geochemistry of A-type granites in the Huangshaping polymetallic deposit (South Hunan, China): Implications for granite

evolution and associated mineralization. J. Asian Earth Sci. https://doi.org/10.1016/j.jseaes.2014.03.004.
Li, H., Watanabe, K., Yonezu, K., 2014b. Zircon morphology, geochronology and trace element geochemistry ofthe granites from the Huangshaping polymetallic deposit, South China: Implications for the magmatic evolution and mineralization processes. Ore Geol. Rev. 60, 14–35.
Li, H., Yonezu, K., Watanabe, K., Tindell, T., 2017. Fluid origin and migration of the Huangshaping W-Mo polymetallic deposit, South China: Geochemistry and 40Ar/39Ar geochronology of hydrothermal K-feldspars. Ore Geol. Rev. 86, 117–129.
Li, X.F., Hu, R.Z., Hua, R.M., Ma, D.S., Wu, L.Y., Qi, Y.Q., Peng, J.T., 2013. The Mesozoic syntexis type granite-related Cu–Pb–Zn mineralization in South China. Acta Petrol. Sin. 29 (12), 4037–4050 (in Chinese with English abstract).
Li, X.F., Huang, C., Wang, C.Z., Wang, L.F., 2016. Genesis of the Huangshaping W-Mo–Cu–Pb–Zn polymetallic deposit in Southeastern Hunan Province, China: Constraints from fluid inclusions, trace elements, and isotopes. Ore Geol. Rev. 79, 1–25.
Li, X.H., McCulloch, M.T., 1996. Secular variation in the Nd isotopic composition of Neoproterozoic sediments from the southern margin of the Yangtze Block: evidence for a Proterozoic continental collision in southeast China. Precambr. Res. 76, 67–76.
Li, X.H., Li, Z.X., Li, W.X., Liu, Y., Yuan, C., Wei, G.J., Qi, C.S., 2007. U-Pb zircon, geochemical and Sr–Nd–Hf isotopic constraints on age and origin of Jurassic I- and A-type granites from central Guangdong, SE China: A major igneous event in response to foundering of a subducted flat-slab? Lithos 97, 186–204.
Li, Y.J., Wei, J.H., Chen, H.Y., Tan, J., Fu, L.B., Wu, G., 2012. Origin of the Maoduan Pb–Zn-Mo deposit, eastern Cathaysia Block, China: Geological, geochronological, geochemical, and Sr-Nd-Pb-S isotopic constraints. Miner Deposita 47, 763–780.
Liu, Y.S., Hu, Z.C., Gao, S., Gunther, D., Xu, J., Gao, C.G., Chen, H.H., 2008. In situ analysis of major and trace elements of anhydrous minerals by LA-ICP-MS without applying an internal standard. Chem. Geol. 257, 34–43.
Ma, L.Y., Lu, Y.F., Qu, W.J., Fu, J.M., 2007. Re–Os isotopic chronology of molybdenites in Huangshaping lead–zinc deposit, southeast Hunan, and its geological implications. Mineral Deposits 26 (4), 425–431 (in Chinese with English abstract).
Mao, J.W., Cheng, Y.B., Chen, M.H., Pirajno, F., 2013. Major types and time-space distribution of Mesozoic ore deposits in South China and their geodynamic settings. Miner Deposita 48, 267–294.
Megaw, P.K.M., Ruiz, J., Titley, S.R., 1988. High-temperature, carbonate-hosted Ag–Pb–Zn(Cu) deposits of northern Mexico. Econ. Geol. 83, 1856–1885.
Meinert, L.D., Dipple, G.M., Nicolescu, S., 2005. World Skarn Deposits. Economic Geology 100th anniversary volume, 299–336.
Meng, Y.M., Hu, R.Z., Huang, X.W., Gao, J.F., Sasseville, C., 2019. The origin of the carbonate-hosted Huize Zn–Pb–Ag deposit, Yunnan province, SW China: constraints from the trace element and sulfur isotopic compositions of pyrite. Mineral. Petrol. 113, 369–391.
Minning, D.A.C., 1981. The effect of fluorine on liquidus phase relationships in the system Qz-Ab-Or with excess water at 1 kb. Contrib. Mineral Petrol. 76, 206–215.
Mukherjee, I., Large, R.R., Bull, S., Gregory, D.G., Stepanov, A.S., Ávila, J., Ireland, T.R., Corkrey, R., 2019. Pyrite trace-element and sulfur isotope geochemistry of paleo-mesoproterozoic McArthur Basin: Proxy for oxidative weathering. Am. Mineral. 104, 1256–1272.
Mungall, J.E., Brenan, J.M., Godel, B., Barnes, S.J., Gaillard, F., 2015. Transport of metals and sulphur in magmas by flotation of sulphide melt on vapour bubbles. Nat. Geosci. 8, 216–219.
Nadeau, O., Willians-Jones, A.E., Stix, J., 2010. Sulphide magma as a source of metals in arc-related magmatic hydrothermal ore fluids. Nat. Geosci. 3, 501–505.
Oliver, N.H.S., McLellan, J.G., Hobbs, B.E., Cleverley, J.S., Ord, A., Feltrin, L., 2006. Numerical models of extensional deformation, heat transfer, and fluid flow across basement-cover interfaces during basin-related mineralization. Econ. Geol. 101, 1–31.
Palinkaš, S.S., Palinkaš, L.A., Renge, C., Spangenberg, J.E., Lüders, V., Molnar, F., Maliqi, G., 2013. Metallogenic Model of the Trepča Pb-Zn-Ag Skarn Deposit, Kosovo: Evidence from Fluid Inclusions, Rare Earth Elements, and Stable Isotope Data. Econ. Geol. 108, 135–162.
Pokrovski, G.S., Borisova, A.Y., Harrichoury, J.C., 2008. The effect of sulfur on vapor-liquid fractionation of metals in hydrothermal systems. Earth Planet. Sci. Lett. 266, 345–362.
Qi, F.Y., Zhang, Z., Zhu, X.Y., Li, Y.S., Zhen, S.M., Gong, F.Y., Gong, X.D., He, P., 2012. Skarn geochemistry of the Huangshaping W-Mo polymetallic deposit in Hunan and its geological significance. Geol. China 39, 338–348 (in Chinese with English abstract).
Raymond, O.L., 1996. Pyrite composition and ore genesis in the Prince Lyell copper deposit, Mt. Lyell mineral field, western Tasmania, Australia. Ore Geol. Rev. 10, 231–250.
Samson, I.M., Williams-Jones, A.E., Ault, K.M., Gagnon, J.E., Fryer, B.J., 2008. Source of fluids forming distal Zn–Pb–Ag skarns: Evidence from laser ablation-inductively coupled plasma-mass spectrometry analysis of fluid inclusions from El Mochito, Honduras. Geology 36 (12), 947–950. https://doi.org/10.1130/G25214A.1.
Seyfried Jr., W.E., Ding, K., 1993. The effect of redox on the relative solubilities of copper and iron in Cl-bearing aqueous fluids at elevated temperatures and pressures: an experimental study with application to subseafloor hydrothermal systems. Geochim. Cosmochim. Acta 57, 1905–1917.
Seyfried Jr., W.E., Ding, K., 1995. Phase equilibria in subseafloor hydrothermal systems: a review of the role of redox, temperature, pH and dissolved Cl on the chemistry of hot spring fluids at mid-ocean ridges. Geophys. Monogr. 91, 248–272.
Shao, Y.J., Wang, W.S., Liu, Q.Q., Zhang, Y., 2018. Trace element analysis of pyrite from the Zhengchong gold deposit, northeast Hunan Province, China: implications for the ore-forming process. Minerals 8 (262), 1–22. https://doi.org/10.3390/min8060262.
Shu, Q.H., Lai, Y., Sun, Y., Wang, C., Meng, S., 2013. Ore genesis and hydrothermal evolution of the Baiyinnuo'er zinc-lead skarn deposit, northeast China: Evidence from isotopes (S, Pb) and fluid inclusions. Econ. Geol. 108, 835–860.
Sun, W.D., Arculus, R.J., Kamenetsky, V.S., Binns, R.A., 2004. Release of gold-bearing fluids in convergent margin magmas prompted by magnetite crystallization. Nature 431, 975–978.
Sun, W.D., Liang, H.Y., Ling, M.X., Zhan, M.Z., Ding, X., Zhang, H., Yang, X.Y., Li, Y.L., Ireland, T.R., Wei, Q.R., Fan, W.M., 2013. The link between reduced porphyry copper deposits and oxidized magmas. Geochim. Cosmochim. Acta 103, 263–275.
Thomas, H.V., Large, R.R., Bull, S., W., Maslennikov, V., Berry, R.F., Fraser, R., Froud, S., Moye, R.,, 2011. Pyrite and pyrrhotite textures and composition in sediments, laminated quartz veins, and reefs at Bendigo gold mine, Australia: insights for ore genesis. Econ. Geol. 106, 1–31.
Tong, Q.M., 1986. The characteristics of metallogeny of the Huangshaping lead-zinc ore deposit of southern Hunan. Geol. Rev. 32 (6), 565–577 (in Chinese with English abstract).
Townley, B.K., Godwin, C.I., 2001. Isotope characterization of lead in galena from ore deposits of Aysen Region, southern Chile. Miner Deposita 36, 45–57.
Vikre, P.G., Poulson, S.R., Alan, E.K., 2011. Derivation of S and Pb in Phanerozoic intrusion-related metal deposits from Neoproterozoic sedimentary pyrite, Great Basin, United States. Econ. Geol. 106, 883–912.
Von Damm, K.L., 1990. Seafloor hydrothermal activity black smoker chemistry and chimneys. Annu. Rev. Earth Planet. Sci. Lett. 18, 173–204.
Wang, C.M., Zhang, D., Wu, G.G., Santosh, M., Zhang, J., Xu, Y.G., Zhang, Y., Y.,, 2014. Geological and isotopic evidence for magmatic-hydrothermal origin of the Ag–Pb–Zn deposits in the Lengshuikeng District, east-central China. Miner Deposita 49, 733–749.
Wang, Y.J., Fan, W.M., Sun, M., Liang, X.Q., Zhang, Y.H., Peng, T.P., 2007. Geochronological, geochemical and geothermal constraints on petrogenesis of the Indosinian peraluminous granites in the south China block: A case study in the Hunan province. Lithos 96, 475–502.
Webster, J.D., Holloway, J.R., Hervig, R.L., 1987. Phase equilibria of a Be, U and F-enriched vitrophyre from Spor Mountain, Utah. Geochem. Cosmochim. Acta 51, 389–402.
Wilkinson, J.J., 2013. Triggers for the formation of porphyry ore deposits in magmatic arcs. Nat. Geosci. 6, 917–925.
Xi, C.Z., Dai, T.G., Liu, W.H., 2009. Lead and sulfur isotope geochemistry of the Huangshaping lead-zinc deposit, Hunan province. Acta Geosci. Sin. 30 (1), 89–94 (in Chinese with English abstract).
Xie, L.W., Zhang, Y.B., Zhang, H.H., Sun, J.F., Wu, F.y.,, 2008. In situ simultaneous determination of trace elements, U-Pb and Lu-Hf isotopes in zircon and baddeleyite. Chin. Sci. Bull. 53, 1565–1573.
Xie, Y.C., Lu, J.J., Ma, D.S., Zhang, R.Q., Gao, J.F., Yao, Y., 2013. Origin of porphyritic granodiorite and mafic microgranular enclave in the Baoshan Pb–Zn polymetallic deposit, southern Hunan Province: Zircon U-Pb chronological, geochemical and Sr–Nd–Hf isotopic constraints. Acta Petrol. Sin. 29 (12), 4186–4214 (in Chinese with English abstract).
Xie, Y.C., Lu, J.J., Yang, P., Ma, D.S., Xu, Z.W., Zhang, R.Q., Cai, Y., Ding, T., 2015. S, Pb, C and O isotopic characteristics and sources of metallogenic materials of Baoshan Pb–Zn deposit, southern Huanan Province. Mineral Deposits 34 (2), 333–351 (in Chinese with English abstract).
Yao, J.M., Hua, R.M., Lin, J.F., 2005. Zircon LA-ICPMS U-Pb dating and geochemical characteristics of Huangshaping granite in southeast Hunan province, China. Acta Petrol Sin. 21 (3), 688–696 (in Chinese with English abstract).
Yao, J.M., Hua, R.M., Qu, W.J., Qi, H.W., Lin, J.F., Du, A.D., 2007. Re–Os isotope dating of molybdenites in the Huangshaping Pb–Zn–W–Mo polymetallic deposit, Hunan Province, South China and its geological significance. Sci. China (Series D) 50, 519–526.
Yao, Y., Chen, J., Lu, J.J., Wang, R.C., Zhang, R.Q., 2014. Geology and genesis of the Hehuaping magnesian skarn-type cassiterite-sulfide deposit, Hunan Province, Southern China. Ore Geol. Rev. 58, 163–184.
Yao, Y., Chen, J., Lu, J.J., Zhang, R.Q., 2013. Geochronology, Hf isotopic compositions and geochemical characteristics of Xitian A-type granite and its geological significance. Mineral Deposits 32 (3), 467–488 (in Chinese with English abstract).
Yuan, S.D., Peng, J.T., Shen, N.P., 2007. 40Ar–39Ar isotopic dating of the Xianghualing Sn-polymetallic orefield in Southern Hunan, China and its geological implications. Acta Geol. Sin. 81 (2), 278–286 (in Chinese with English abstract).
Yuan, Y.B., Yuan, S.D., Chen, C.J., Huo, R., 2014. Zircon U-Pb ages and Hf isotopes of the granitoids in the Huangshaping mining area and their geological significance. Acta Petrol. Sin. 30, 64–78 (in Chinese with English abstract).
Yuan, Z.X., Wu, L.S., Zhang, Z.Q., Ye, X.J., 1991. Study on Sm–Nd and Rb–Sr isotopic age of the Mayuan group in northern Fujian. Acta Petrol. Mineral. 10, 127–132 (in Chinese with English abstract).
Zhang, J., Deng, J., Chen, H.Y., Yang, J.Q., Cooke, D.R., Danyushevskiy, L., Gong, Q.J., 2014. LA-ICP-MS trace element analysis of pyrite from the Chang'an gold deposit, Sanjiang region, China: implication for ore-forming process. Gandwana Res. 26 (2), 557–575.
Zhang, R.Q., 2014. Petrogenesis and metallogeny of the W- and Sn-bearing granites in southern Hunan province: Case study from Wangxianling and Xintianling. (Ph.D. thesis). Nanjing University, Nanjing, pp. 1–193 (in Chinese with English abstract).
Zhou, X.M., Sun, T., Shen, W.Z., Shu, L.S., Niu, Y.L., 2006. Petrogenesis of Mesozoic granitoids and volcanic rocks in South China: A response to tectonic evolution. Episodes 29 (1), 26–33.
Zhu, C.W., Liao, S.L., Wang, W., Zhang, Y.X., Yang, T., Fan, H.F., Wen, H.J., 2018. Variations in Zn and S isotope chemistry of sedimentary sphalerite, Wusihe Zn-Pb deposit, Sichuan Province, China. Ore Geol. Rev. 95, 639–648.

Zhu, C.W., Wen, H.J., Zhang, Y.X., Fan, H.F., 2016. Cadmium and sulfur isotopic compositions of the Tianbaoshan Zn-Pb-Cd deposit, Sichuan Province, China. Ore Geol. Rev. 76, 152–162.
Zhu, X.Y., Wang, J.B., Wamg, Y.L., Cheng, X.Y., Fu, Q.B., 2012. Sulfur and lead isotope constraints on ore formation of the Huangshaping W-Mo–Bi–Pb–Zn polymetallic ore deposit, Hunan Province, South China. Acta Petrol. Sin. 28 (12), 3809–3822 (in Chinese with English abstract).
Zuo, C.H., Lu, R., Zhao, Z.X., Xu, Z.W., Lu, J.J., Wang, R.C., Chen, J.Q., 2014. Characterization of element geochemistry, LA–ICP–MS zircon U-Pb age, and Hf isotope of granodiorite in the Shuikoushan deposit, Changning, Hunan Province. Geol. Rev. 60 (4), 811–823 (in Chinese with English abstract).